Bioorganic Chemistry 85 (2019) 253–273

Contents lists available at ScienceDirect

Bioorganic Chemistry

journal homepage: www.elsevier.com/locate/bioorg

Synthesis, anticancer effect and molecular modeling of new thiazolylpyrazolyl coumarin derivatives targeting VEGFR-2 kinase and inducing cell cycle arrest and apoptosis

Tahia K. Mohamed[a], Rasha Z. Batran[a,*], Samia A. Elseginy[b], Mamdouh M. Ali[c], Abeer E. Mahmoud[c]

[a] Chemistry of Natural Compounds Department, Pharmaceutical and Drug Industries Research Division, National Research Centre, 33 El Bohouth St., Dokki, P.O. Box 12622, Giza, Egypt
[b] Green Chemistry Department, Chemical Industries Research Division, National Research Centre, 33 El Bohouth St., Dokki, P.O. Box 12622, Giza, Egypt
[c] Biochemistry Department, Division of Genetic Engineering and Biotechnology, National Research Centre, 33 El Bohouth St., Dokki, P.O. Box 12622, Giza, Egypt

ARTICLE INFO

Keywords:
Coumarin
Thiazolylpyrazoline
Anticancer
VEGFR-2
Apoptosis
Molecular modeling

ABSTRACT

New thiazolylpyrazolyl coumarin derivatives were synthesized and tested for their anticancer potential *in vitro* against five different human cell lines, including breast MCF-7, lung A549, prostate PC3, liver HepG2 and normal melanocyte HFB4. Breast carcinoma revealed higher sensitivity towards compounds **7a, 8c, 9b, 9c** and **9d** with IC_{50} values ranging from 5.41 to 10.75 μM in comparison to the reference drug doxorubicin (IC_{50} = 6.73 μM). In addition, no noticeable toxicity was exhibited towards normal cells HFB4. Moreover, *in vitro* studies of the VEGFR-2 inhibition in human breast cancer MCF-7 cell line for the promising cytotoxic compounds showed that compounds **7a, 8c, 9b, 9c** and **9d** were potent inhibitors at low micromolar concentrations (IC_{50} = 0.034–0.582 μM) compared to the reference drug, sorafenib (IC_{50} = 0.019 μM). Several theoretical and experimental studies were done to reveal the molecular mechanisms that control breast carcinoma metastasis. The mechanistic effectiveness in cell cycle progression, apoptotic induction and gene regulation were assessed for the promising compound **9d** due to its remarkable cytotoxic activity against MCF-7 and significant VEGFR-2 inhibition. Flow cytometeric analysis showed that compound **9d** induced cell growth cessation at G2/M phase and increased the percentage of cells at pre-G1 phase that stimulates the apoptotic death of MCF-7 cells. Furthermore, real time PCR assay illustrated that compound **9d** up regulated p53 gene expression and elevated Bax/Bcl-2 ratio which confirmed the mechanistic pathway of compound **9d**. Moreover, the apoptotic induction of breast cancer cells MCF-7 was enhanced effectively through activation of caspases-7 and 9 by compound **9d**. On the other hand, a set of *in silico* methods such as molecular docking, molecular dynamics simulation, QSAR analysis as well as ADMET analysis was performed in order to study the protein-ligand interactions and the relationship between the physicochemical properties and the inhibitory activity of the promising compounds **7a**, **8c** and **9d**. Based on the aforementioned findings, compound **9d** could be considered as effective apoptosis modulator and promising lead for future development of new anti-breast cancer agents.

1. Introduction

Cancer is one of the most complex and serious health disorders in the world. The global burden of cancer and mortality are increasing tremendously [1]. Recently, targeted cancer therapies have been approved for the treatment of specific cancers as breast, lung, colorectal, and pancreatic cancers, as well as leukemia, lymphoma, and multiple myeloma. These cytotoxic therapies prevent cancer cells proliferation by interfering with specific molecules required for tumor growth and development as such, they reduce the adverse effects of other classical non-selective chemotherapies and overcome the resistance developed by the existing anticancer remedies [2]. Targeted chemotherapy encompasses various approaches amongst them is inhibition of angiogenesis that has proven to be an attractive strategy for hindering tumor growth [3].

Angiogenesis is a vital physiological process occurring during embryogenesis, inflammation and wound healing.[4]. However, in pathological angiogenesis new blood vessels infiltrate tumor masses and

* Corresponding author.
E-mail address: rasha_batran@yahoo.com (R.Z. Batran).

https://doi.org/10.1016/j.bioorg.2018.12.040
Received 22 October 2018; Received in revised form 31 December 2018; Accepted 31 December 2018
Available online 03 January 2019

supply them with oxygen and nutrients enhancing tumor progression and metastasis [5]. Hence, inhibition of angiogenesis is effective well-tolerated strategy in preventing tumor growth with lower adverse effects than other traditional chemotherapies [3].

A wide variety of growth factors are implicated in the angiogenic process. Vascular endothelial growth factor family (VEGFs) is the one of the most specific and crucial signaling proteins in both physiological and pathological angiogenesis [6]. These angiogenic ligands are extremely expressed in various types of human cancer cells [7]. They not only stimulate angiogenesis but also they can suppress the antitumor immune response, so reduce the ability of the host immune system to eradicate tumor cells [8].

VEGFs exert their angiogenic effects *via* interaction with the kinase domain of vascular endothelial growth factor receptors (VEGFRs). VEGF family of tyrosine kinase receptor (VEGFR-TK) includes three protein receptors; VEGFR-1 (FLT1), VEGFR-2 (KDR/FLK1) and VEGFR-3 (FLT4). VEGFR1 and VEGFR-2 mediate angiogenesis while VEGFR-3 mostly regulates lymphangiogenesis [9,10]. Suppression of VEGF/VEGFR signaling pathway is considered as an interesting therapeutic target for inhibiting tumor angiogenesis and the following tumor growth [11].

VEGFR-2, is a type of III transmembrane receptor tyrosine kinase (RTK) expressed in various cancer cells and mediates almost all the cellular responses to VEGF representing an essential target among the angiogenesis-related kinases, thus, regarded as the most substantial transducer of VEGF-dependent angiogenesis [7,12,13]. Blocking or down regulation of VEGFR-2 signaling became a fundamental approach for the discovery and development of new drugs for numerous human angiogenesis-dependent cancers [14].

Over the past few years, a diverse range of VEGFR-2 suppressors have been developed and approved by the FDA as anti-angiogenic drugs for the treatment of different types of solid tumors like anti-VEGF monoclonal antibodies; e.g., bevacizumab [15], and VEGFRs inhibitors as sorafenib, sunitinib and regorafenib [16]. However, the adverse effects associated with some anti-VEGF agents encourage the development of safer VEGFR-2 inhibitors [17].

VEGFR-2 inhibitors target the ATP binding site of the RTKs thus they are classified into three types according to the mode of binding to the ATP binding pocket [18]. Type I inhibitors bind to the active “DFG-in” conformation through hydrogen bond formation in the hinge region and hydrophobic interactions in the adenine region. Type II inhibitors act on ATP binding pocket and function in the adjacent non-conserved allosteric hydrophobic site in the inactive “DFG-out”conformation [19,20]. Type III inhibitors adopt the inactive “DFG-out” conformation and bind entirely beyond the gatekeeper residue to the less conserved allosteric site outside the ATP binding site [21,22].

Many plant-derived constituents play a very dominant role in the contemporary cancer therapy, such as paclitaxel (taxol®) [23], vinblastine (velban®) [24], vincristine (oncovin®) [24] and irinotecan (camptosar®) [25]. The prevention of cancer using naturally derived compounds has been estimated as an integral aspect for cancer control [26].

A perusal of the literature revealed that the benzopyrone scaffold constitutes an important part of various natural products and bioactive molecules. Quercetin (4*H*-benzopyran-4-one compound) has been estimated as potential anticancer agent targeting VEGFR-2 [27]. Chebulagic acid, a benzopyran tannin isolated from *Terminalia chebula* fruits, inhibited VEGFR-2 phosphorylation and exhibited anti-angiogenic properties through blocking the VEGF-VEGFR-2 complex and cell-cell contact dependent downstream signaling pathways [28]. Moreover, the anti-angiogenic activity of the synthetic benzopyran KR-31831was attributed to down regulation of VEGFR-2 expression (Fig. 1) [29].

Indeed, coumarin derivatives (2*H*-benzopyran-2-ones) have attracted great attention owing to their diverse biological properties, especially as chemotherapeutic candidates [30–35]. Recent studies showed that a number of naturally occurring and synthetic coumarin compounds exhibit antiproliferative activity *via* inhibition of VEGFR-2 mediated signaling pathways (Fig. 1) [34–38].

Among the currently identified antitumor scaffolds, thiazolylpyrazolines represent an important class of compounds with promising cytotoxic effects [39,40] and RTKs suppressing potential [41–43] (Fig. 2).

Hybridization of two or more scaffolds in a single molecule provides a favorable hybrid pharmacophore approach for the development of new anticancer candidates. With this aspect in mind and in an effort to develop new cytotoxic candidates based on the naturally derived coumarin scaffold, we synthesized a set of new coumarin derivatives conjugated with thiazolyl pyrazoline moiety as potential VEGFR-2 inhibitors taking in consideration the influence of molecular orientation, ring size variation and the presence of heteroatoms that could provide hydrogen bonding interactions with VEGFR-2 binding pocket (Fig. 3). The anticancer activity against four cancer cell lines; MCF7 (breast) A549 (lung), PC3 (prostate) and HepG2 (liver) carcinoma cell lines was evaluated in addition to normal melanocyte HFB4. Moreover, *in vitro* evaluation of the synthesized compounds for their inhibitory effect against VEGFR-2 was carried out. The mechanistic pathways of the anticancer activity were also assessed for the most potent compound to perform extra investigations such as cell cycle analysis and apoptosis markers.

Molecular modeling studies were performed to find out the mode of interaction between the promising target compounds and the key amino acids of VEGFR-2 (hot spots) in addition to evaluate their binding stability and explore the relationship between the physicochemical properties and the inhibitory effects aiming to furnish a framework for optimizing the efficacy and selectivity of the inhibitors in a rational manner.

2. Results and discussion

2.1. Chemistry

The target thiazolylpyrazolyl coumarin derivatives **3–9** were synthesized following the general procedures outlined in Schemes 1–4.

Initially, 4-dimethylaminophenyl chalcone compounds **1a,b** were synthesized through base catalyzed Claisen Schmidt condensation of 3-acetylcoumarin and /or 3-acetyl-4-hydroxycoumarin with 4-dimethylaminophenyl benzaldehyde [44,45]. Hetrocyclization of chalcones **1a,b** with thiosemicarbazide in the presence of a catalytic amount of conc. HCl afforded the thiocarbamoyl pyrazoline derivatives **2a,b.**

The thiazolylpyrazoline derivatives **3–8** were obtained *via* condensation of the coumarinyl thiocarbamoylpyrazolines **2a**,**b** with different α-haloketones through *S*-alkyalation and subsequent water or alcohol molecule elimination.

The 4-methyl/phenylthiazolyl pyrazoline derivatives **3a**,**b** and **4a**,**b** were obtained by refluxing the intermediates **2a,b** with chloroacetone and /or phenacyl bromide, respectively, in ethanol using a catalytic amount of anhydrous sodium acetate. Similarly, cyclocondensation of the key intermediates **2a**,**b** with ethyl-2-chloroacetoacetate under the same conditions yielded the corresponding ethyl-2-pyrazolyl-4-methylthiazole-5-carboxylate compounds **5a,b** in a good yield (Scheme 1).

The pyrazolyl thiazolidinones **6a**,**b** and **7a**,**b** were prepared upon treatment of **2a,b** with ethylbromoacetate and/ or ethyl 2-bromopropionate, respectively, in refluxing ethanol in the presence of anhydrous sodium acetate (Scheme 2).

The target compounds **8a–d**, were synthesized *via* one pot heterocyclization reaction of thiocarbamoyl pyrazolines **2a**,**b** and the appropriate hydrazonoyl chlorides in dioxane in the presence of triethylamine under reflux conditions (Scheme 3).

Furthermore, coupling 4-phenylthiazolyl pyrazoline compounds **4a**,**b** with the diazotized 4-toluidine and /or 4-chloroaniline in the presence of sodium acetate trihydrate afforded the corresponding azo derivatives **9a–d** (Scheme 4).

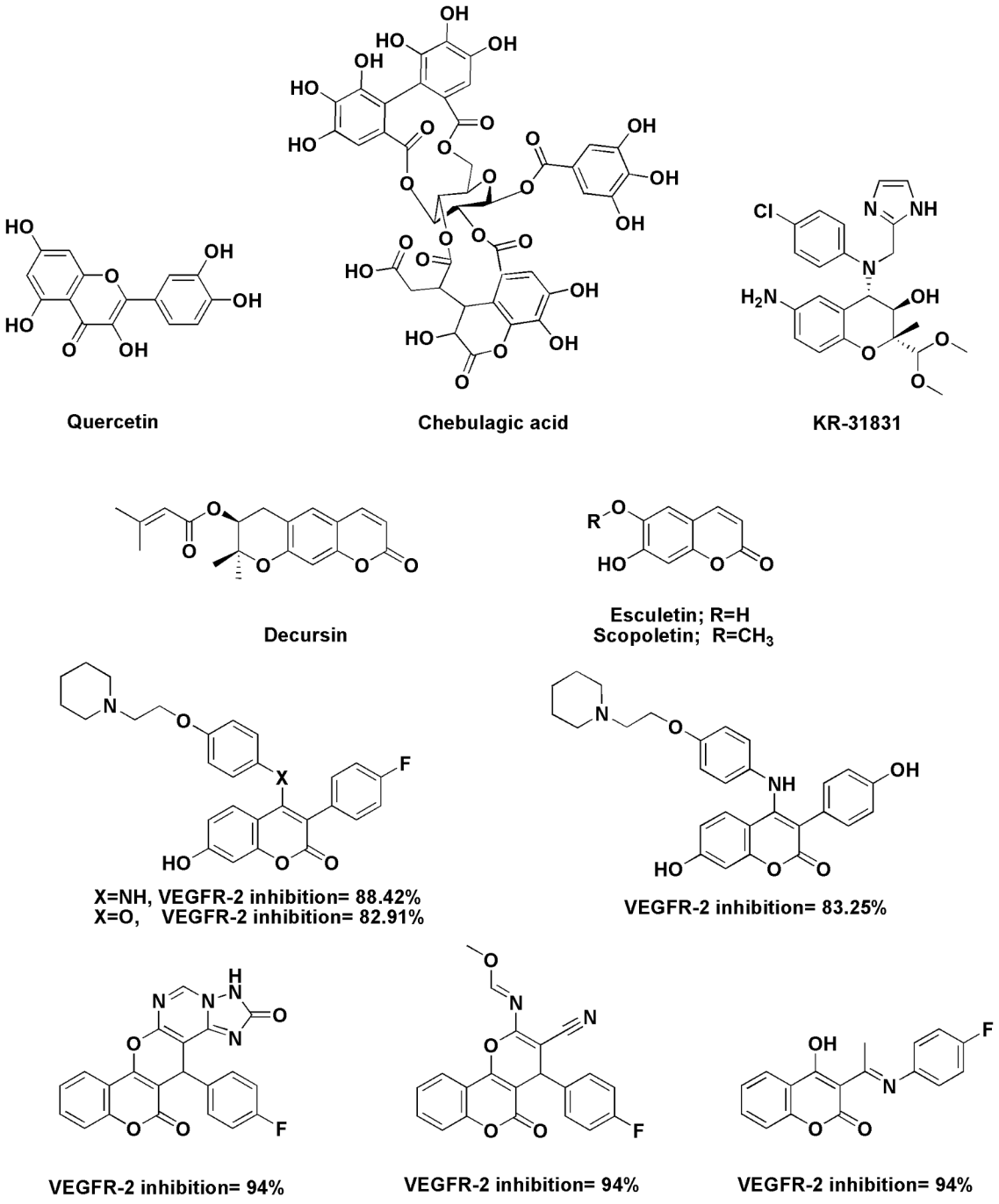

Fig. 1. Examples of different naturally occurring and synthetic benzopyrans as VEGFR-2 inhibitors.

2.2. Biology

2.2.1. In vitro cytotoxic effect

All the synthesized compounds were evaluated for their *in vitro* cytotoxic activity against four human cancerous cell lines; breast MCF-7, lung A549, prostate PC3 and liver HepG2 cancer cells in addition to normal melanocyte HFB4 cells *via* SRB assay and using doxorubicin as a positive control. The cytotoxic effects were expressed by median growth inhibitory concentration (IC_{50}) as shown in Table 1. The results revealed that some of the synthesized compounds were sensitive to MCF-7 cells while all of them did not exert any activity against lung A549, prostate PC3 and HepG2 cancer cells. Compounds **7a**, **8c**, **9b**, **9c** and **9d** were found to be potent and selective anticancer agents against MCF-7 cells with IC_{50} values of 10.75, 8.61, 6.56, 6.51 and 5.41 μM respectively versus 6.73 μM for the reference drug doxorubicin. Compounds **4b, 5b** and **8d** revealed moderate activities with IC_{50} values of 23.40, 19.96 and 16.53 μM, respectively compared to doxorubicin. In addition, the effect of the synthesized compounds on the toxicity of normal HFB4 cells revealed that the aforementioned promising compounds **4b, 5b, 7a**, **8c**, **8d**, **9b**, **9c** and **9d** showed no noticeable activity against HFB4 cells.

2.2.2. Structure activity relationship of the synthesized compounds against MCF-7 cells

Both the parent coumarinyl thiocarbamoyl pyrazolines **2a** and **2b** showed no activity against MCF-7. While the cyclized 4-methylthiazolyl pyrazolines **3a** and **3b** and the 4-phenylthiazolyl pyrazoline compound **4a** displayed diminished effectiveness (IC_{50} = 85.57–165.96 μM),

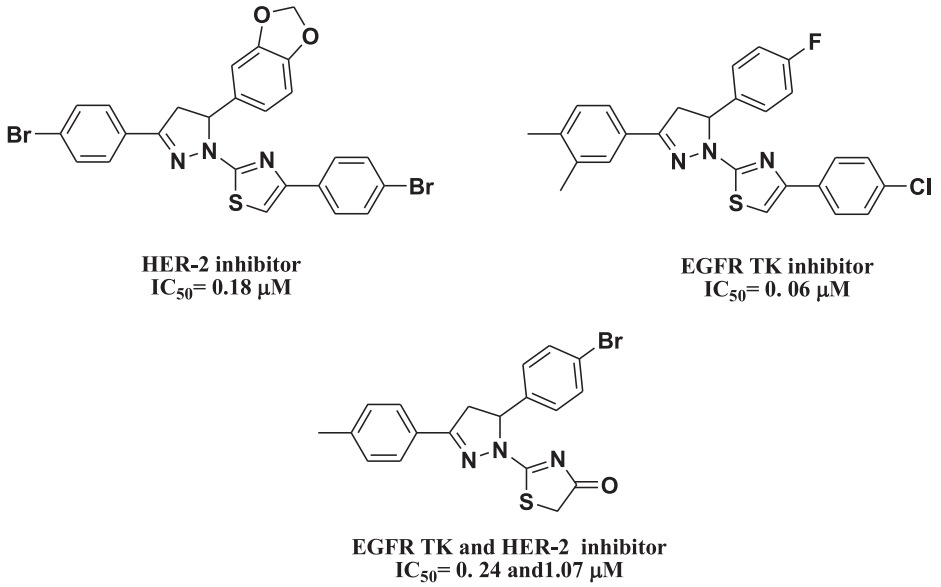

Fig. 2. Examples of different thaizolylpyrazoline compounds as RTK inhibitors.

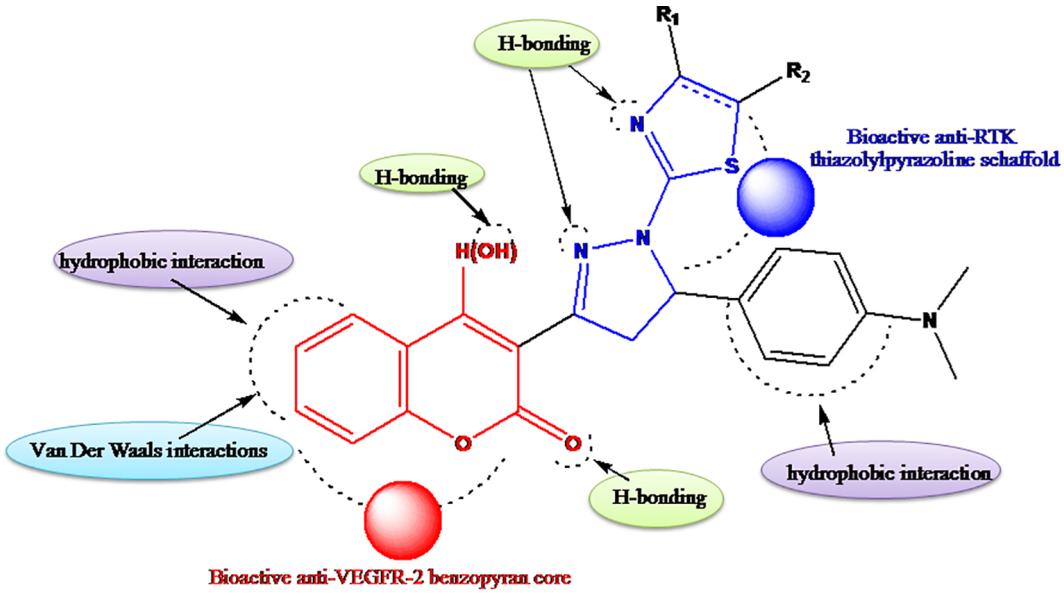

Fig. 3. Proposed hypothetic model for thiazolylpyrazolyl coumarin compounds.

compound **4b** showed improved activity against MCF-7 cells (IC_{50} = 23.40 µM). The introduction of ethylcarboxylate group in the 5-position of the 4-methylthiazole moiety, compounds **5a** and **5b**, greatly ameliorated the cytotoxic effect (IC_{50} = 58.90 and 19.96 µM).

The 5-methylthiazolidinone derivatives of coumarin and 4-hydroxycoumarin **7a** and **7b** (IC_{50} = 10.75 and 67.02 µM) were more potent than the desmethyl derivatives **6a** and **6b** (IC_{50} = 106.36 and 124.19 µM) with compound **7a** being the most potent within the synthesized thiazolidinone series.

The 5-(*p*-chlorophenyldiazenyl)-4-methylthiazolylpyrazoline derivatives of coumarin and 4-hydroxycoumarin **8c** and **8d** (IC_{50} = 8.16 and 16.53 µM) showed higher potency than the *p*-tolyldiazenyl derivatives **8a** and **8b** (IC_{50} = 55.88 and 45.69 µM). Compound **8c** displayed remarkable anticancer effect compared to the reference doxorubicin being 2 folds more cytotoxic than the 4-hydroxycoumarin congener **8d**.

The 5-aryldiazenyl-4-phenylthiazolyl-pyrazoline compounds **9a-d** constitute the most potent series of the synthesized compounds. The 5-(*p*-tolyldiazenyl)-4-phenylthiazolyl-pyrazolyl-4-hydroxycoumarin derivative **9b** and the two 4-chlorophenyldiazenyl derivatives **9c** and **9d** showed significant cytotoxic effects against MCF-7 (IC_{50} = 6.56, 6.51 and 5.41 µM, respectively) with compound **9d** being the most active compound among all the synthesized derivatives (IC_{50} = 5.41 µM) and showing outstanding cytotoxic activity compared to the reference drug doxorubicin (IC_{50} = 6.73 µM).

2.2.3. In vitro effect of the synthesized compounds on the level of VEGFR-2 in MCF-7 cell line

It was investigated that VEGFR-2 is highly expressed in breast cancer cells [46]. Up-regulation of VEGFR-2 mRNA was detected in early stages of primary and metastatic invasive breast cancers [47]. Targeting VEGFR-2 over-expression in breast cancer cells could be an efficacious trend for developing new therapeutic anti-breast cancer modalities. Consequently, *in vitro* study was done to assay the level of human VEGFR-2 in MCF-7 cells for eight compounds **4b**, **5b**, **7a**, **8c**, **8d**, **9b**, **9c** and **9d** which displayed the most potent cytotoxic effect against

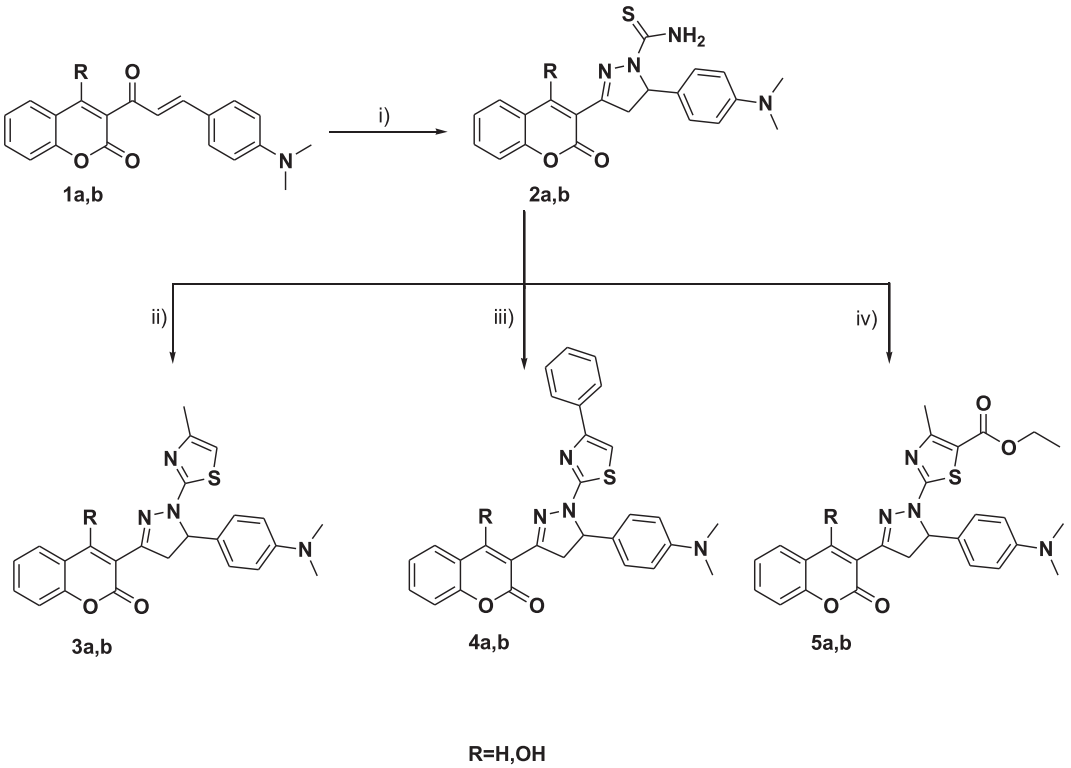

Scheme 1. (i) $NH_2CSNHNH_2$, EtOH, HCl, reflux, (ii) CH_3COCH_2Cl, CH_3COONa, EtOH, reflux, (iii) $PhCOCH_2Br$, CH_3COONa, EtOH, reflux, (iv) $CH_3COCH(Cl)COOC_2H_5$, CH_3COONa, EtOH, reflux.

MCF-7 where the cells were treated with 20 µL of IC_{50} values of the compounds (Table 2). The results indicated that compounds **7a, 8c, 9b, 9c** and **9d** showed significant reduction in VEGFR-2 level with percentage of inhibition values 82, 80, 84, 87 and 85% respectively as compared to the control untreated cancer cells. These results were consistent with the cytotoxic effect against MCF-7 cell line where these compounds exhibited excellent anticancer activity against MCF-7 which indicates that the potential anticancer effect of the target compounds could be attributed to suppression of VEGFR-2 gene expression. Otherwise, compounds **4b**, **5b** and **8d** exhibited moderate reduction in VEGFR-2 level with percentage of inhibition values 57, 60 and 56% respectively, as shown in Table 2.

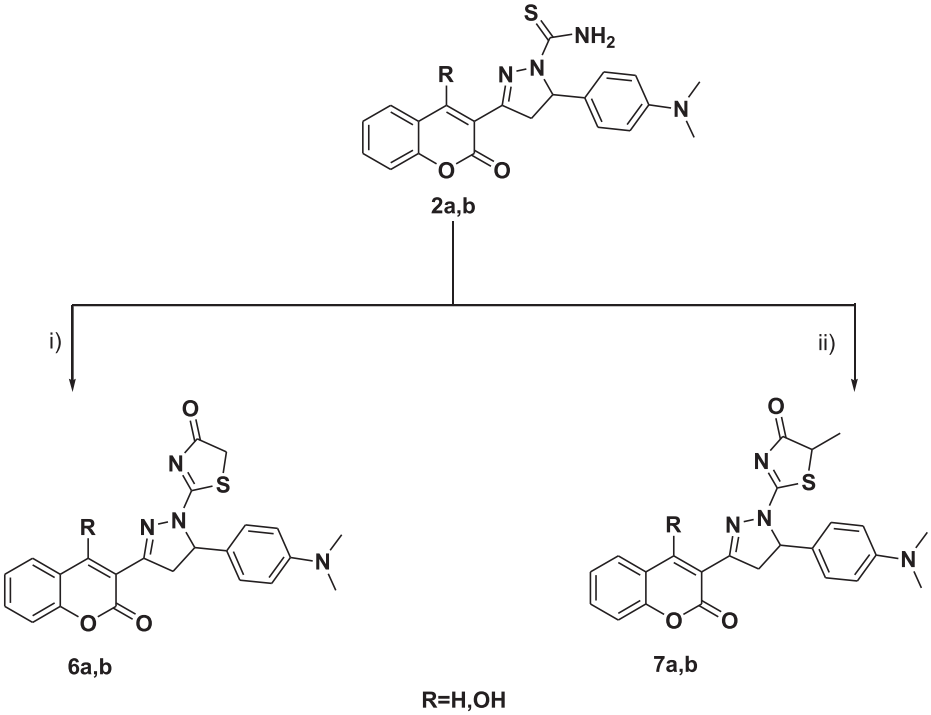

Scheme 2. (i) $BrCH_2COOC_2H_5$, CH_3COONa, EtOH, reflux. (ii) $CH_3CH(Br)COOC_2H_5$, CH_3COONa, EtOH, reflux.

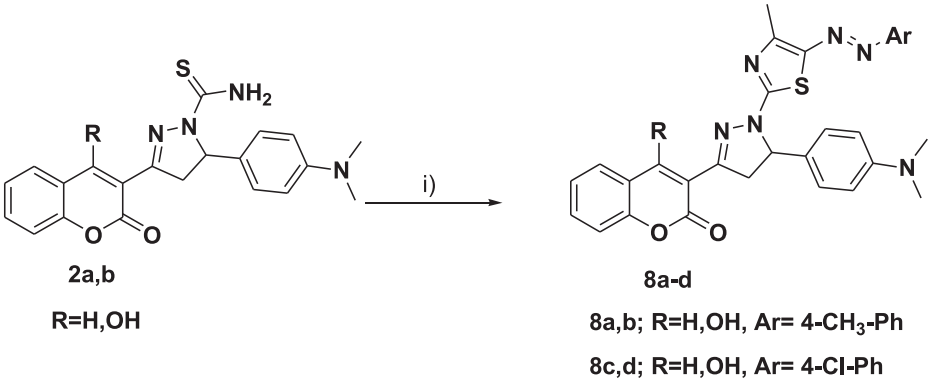

Scheme 3. (i) $CH_3CO(Cl)C{=}NNHAr$, Dioxane, Et_3N, reflux.

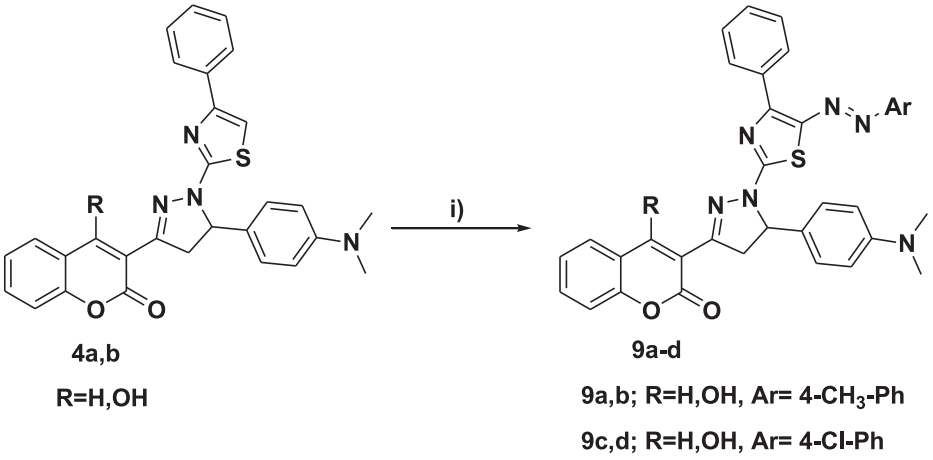

Scheme 4. (i) ArN_2Cl, EtOH, $CH_3COONa{\cdot}3H_2O$.

Table 1
The anticancer activity of the synthesized compounds **(2–9)** on MCF-7 and HFB4 cell lines.

Compounds	IC_{50} μM (μg/ml)*	
	MCF-7	Normal HFB4
2a	160.62 (63.00 ± 7.14)	27.59 (10.83 ± 1.80)
2b	163.29 (66.70 ± 7.50)	35.03 (14.31 ± 2.14)
3a	165.96 (71.45 ± 8.12)	37.35 (16.08 ± 1.76)
3b	85.57 (38.21 ± 3.77)	30.91 (13.80 ± 2.06)
4a	98.05 (48.30 ± 5.50)	31.97 (15.75 ± 2.30)
4b	23.40 (11.90 ± 3.77)	119.55 (60.80 ± 8.12)
5a	58.90 (29.60 ± 4.11)	61.94 (31.13 ± 4.40)
5b	19.96 (10.35 ± 1.50)	130.68 (67.77 ± 6.50)
6a	106.36 (46.00 ± 6.30)	44.63 (19.30 ± 2.20)
6b	124.19 (55.70 ± 4.90)	26.20 (11.75 ± 1.70)
7a	10.75 (4.80 ± 0.47)	163.15 (72.85 ± 9.10)
7b	67.02 (31.00 ± 4.32)	41.08 (19.00 ± 2.38)
8a	55.88 (30.66 ± 5.15)	38.55 (21.15 ± 3.00)
8b	45.69 (25.80 ± 3.90)	32.25 (18.21 ± 2.07)
8c	8.61 (4.90 ± 0.50)	135.31 (77.00 ± 8.80)
8d	16.53 (9.67 ± 1.10)	122.89 (71.90 ± 9.10)
9a	43.88 (26.80 ± 4.11)	31.70 (19.36 ± 3.22)
9b	6.56 (4.11 ± 0.60)	128.60 (80.60 ± 9.50)
9c	6.51 (4.11 ± 0.60)	113.76 (71.80 ± 9.76)
9d	5.41 (3.50 ± 0.50)	127.23 (82.34 ± 10.11)
Doxorubicin	6.73 (3.66 ± 0.42)	163.01 (88.60 ± 11.11)

* The concentration required to produce 50% inhibition of cell growth compared to control experiments. Data were expressed as mean ± standard error (S.E.) of three independent experiments.

2.2.4. IC_{50} determination of the synthesized compounds against VEGFR-2

Compounds **7a**, **8c**, **9b**, **9c** and **9d** which displayed high percentage of inhibition on VEGFR-2 level in MCF-7 cells were further investigated for their inhibitory effect on human VEGFR-2 *via* ELISA and using sorafenib as a positive control to determine their IC_{50} values as shown in Table 3. The tested compounds showed significant inhibitory effect at sub-micromolar concentrations (IC_{50} = 0.034–0.582 μM). It was found that compound **9d** showed the highest inhibition effect towards VEGFR-2 (IC_{50} = 0.034 μM) compared to sorafenib (IC_{50} = 0.019 μM). Compound **8c** showed remarkable effect against VEGFR-2 (IC_{50} = 0.082 μM) while the inhibition potency was reduced for compounds **7a**, **9b** and **9c** (IC_{50} = 0.169, 0.213, 0.582 μM, respectively).

2.2.5. Cellular mechanism of action

2.2.5.1. Cell cycle arrest. Compound **9d**, which showed the most potent cytotoxic effect on MCF-7 and elicited the highest inhibitory activity against VEGFR-2, was selected for further assessment of its cellular mechanism of action concerning cell cycle progression and induction of apoptosis in MCF-7 cells using DNA flow cytometric analysis. MCF-7 cells were treated with compound **9d** at its IC_{50} value of 5.41 μM for 24 h and its impact on normal cell cycle profile and induction of apoptosis was analyzed. Exposure of MCF-7 cells to compound **9d** resulted in an interference with the cell cycle distribution inducing a significant increase in the percentage of cells at pre-G1 by 7.02 folds with synchronous significant arrest in the G2-M phase by 2.12 folds compared to the control (Fig. 4A and B). Accumulation of cells in pre-G1 and G2/M phases is a significant remark of the apoptotic role of compound **9d** in MCF-7 cells.

Table 2
Effect of the most active synthesized compounds on the VEGFR-2 level (pg/ml).

Compounds	VEGFR-2 level (pg/ml)	VEGFR-2 Inhibition* (%)
4b	1983.33 ± 23.18	(57%)
5b	1850.19 ± 21.70	(60%)
7a	836.38 ± 91.11	(82%)
8c	930.80 ± 111.65	(80%)
8d	2060.00 ± 25.12	(56%)
9b	730.90 ± 82.16	(84%)
9c	600.76 ± 73.80	(87%)
9d	685.37 ± 76.11	(85%)
DMSO	4650.75 ± 56.00	–

* Percentage of inhibition values are estimated in comparison to control untreated cells. Data were expressed as mean ± standard error (S.E.) of three independent experiments.

Table 3
IC_{50} values of tested compounds on VEGFR-2.

Compound	IC_{50} (μM) against VEGFR-2*
7a	0.1696 ± 0.0104
8c	0.08154 ± 0.00357
9b	0.21296 ± 0.01433
9c	0.5824 ± 0.02114
9d	0.0344 ± 0.00259
Sorafenib	0.01995 ± 0.00247

* The concentration required to produce 50% inhibition of VEGFR-2 compared to control experiments. Data were expressed as mean ± standard error (S.E.) of three independent experiments.

2.2.5.2. Apoptosis determination by annexin-V assay. To further assure the apoptotic ability of compound **9d**, a flow cytometric analysis was carried out, using dual staining with propidium iodide (PI) and annexin V-FITC which allows discrimination between viable, early apoptotic, late apoptotic and necrotic cells. Propidium iodide stains DNA of late apoptotic and necrotic cells displaying red fluorescence while the labeled protein annexin-V, binds strongly and specifically to phosphatidylserine (PS) which is exposed on the surface of the apoptotic cells and fluoresces green.

After 24 h, MCF-7 cells treated with compound **9d** at its IC_{50} concentration (5.41 μM) displayed a significant decrease in the percentage of surviving cells. Moreover, a significant increase in the late cellular apoptosis was observed (from 0.35% to 6.11% compared to control). In addition, about 6.8 folds increase in the percentage of annexin V-FITC positive apoptotic cells was also detected indicating early apoptosis (Fig. 4C and D).

2.2.5.3. Effect of compound 9d on the level of p53/Bax/ Bcl-2. Apoptosis is triggered in a cell through two major apoptotic pathways, the extrinsic pathway (the death receptor) or the intrinsic pathway (mitochondrial pathway) [48]. Cancer cells can acquire apoptotic resistance by modulating the expression of Bcl-2 family proteins which are responsible for regulating the mitochondrial apoptotic pathway through expressing anti-apoptotic proteins as Bcl-2 or down-regulating pro-apoptotic proteins, such as Bax [49]. The expression of anti-apoptotic Bcl-2 and pro-apoptotic Bax genes is regulated by the tumor suppressor gene p53 [50]. In this study, we assessed the impact of compound **9d** which displayed promising apoptosis inducing activity, on the intrinsic apoptotic pathway *via* measuring the levels

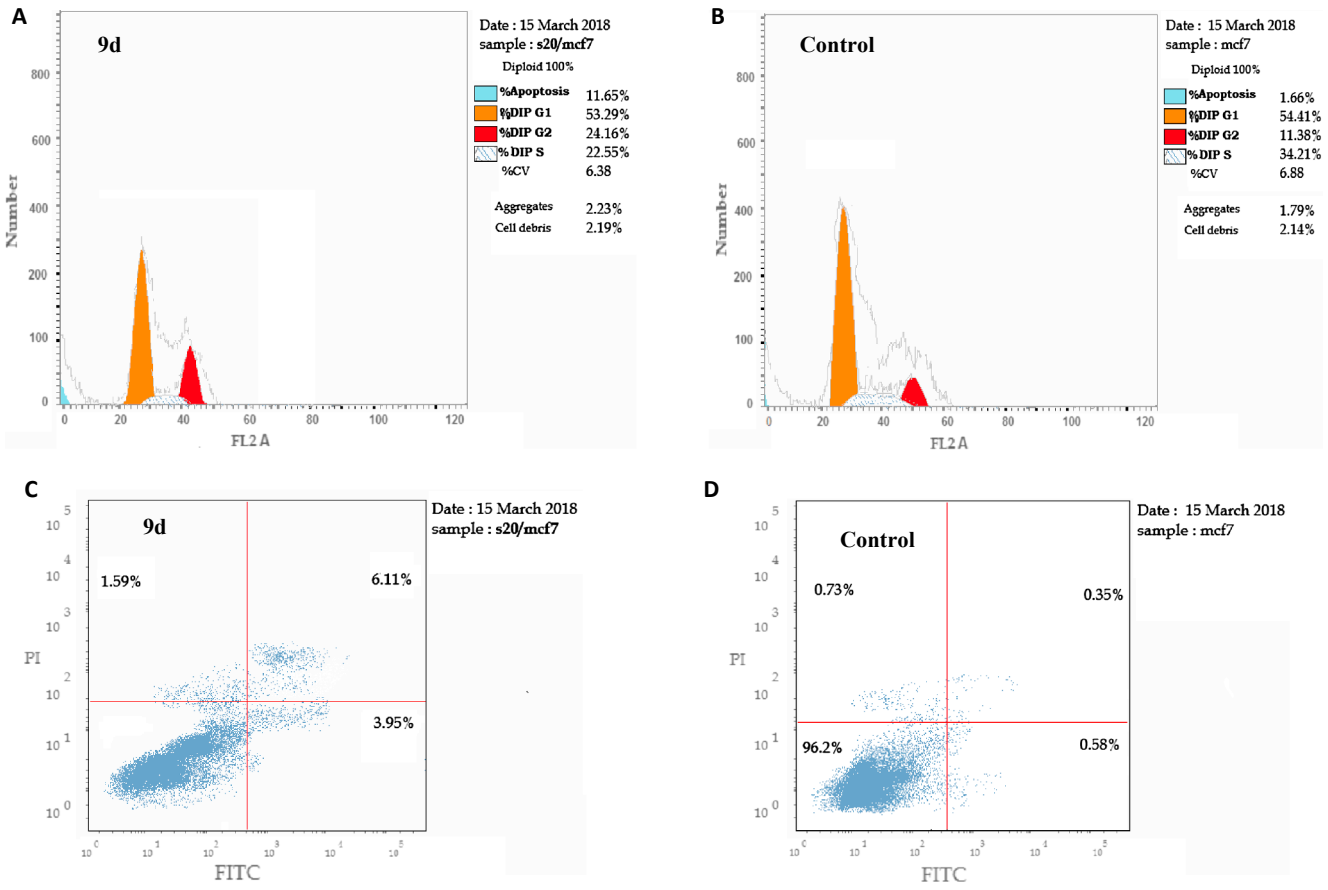

Fig. 4. Cellular mechanism of action of compound **9d**. (A and B) Cell cycle analysis of MCF-7 after incubation with compound **9d** for 24 h. DMSO diluent was used as a control. (C and D) Induction of apoptosis by compound **9d**. Cells were exposed to **9d** for 24 h and analyzed by annexin V/ PI staining. The percentage of cells undergoing apoptosis is defined as the sum of early apoptotic (annexin V+/PI−) cell percentage and late apoptotic (annexin V+/PI+) cell percentage.

Table 4
p53/Bax/BCL-2 analysis results after treatment with compound **9d** for 24 h.

Compound	Conc. (μM)	Bax fld	Bcl2 fld	p53 fld
9d	5.41	7.046391	0.329701	5.952977
Doxorubicin	6.73	8.534015	0.248688	8.187941
Control	–	1	1	1

of p53, Bax and Bcl2 (Table 4).

MCF-7 cells were exposed to compound **9d** at its IC_{50} concentration (5.41 μM) for 24 h. As demonstrated in Table 4, the tested compound **9d** induced a significant increase in the expression of the tumor suppressor gene p53 and the pro-apoptotic protein Bax by 5.95 and 7.05 folds, respectively with concurrent decrease in the expression levels of the anti-apoptotic protein Bcl-2 compared to the control (Table 4). Consequently, a significant elevation in Bax/Bcl-2 ratio was recorded that advocates the ability of compound **9d** to enhance the therapeutic response in the breast cancer MCF-7 cells.

2.2.5.4. Effect of compound 9d on the level of active caspases-7 and -9. The initiation of apoptosis by either the extrinsic or the intrinsic pathways gives rise to a cascade activation of cysteine dependent aspartic acid-specific proteases called caspases. After DNA damage, mitochondrial cytochrome *C* and other pro-apoptotic factors are released into the cytosol and initiate activation of caspase-9. Consequently, the active caspase-9 (initiator caspase) triggers the activation of downstream effector caspases-3 and 7 [51]. The mitochondrial-dependent apoptosis in MCF-7 cells is essentially dependent on caspase-7 activation due to lack of caspase-3.

In the current study, compound **9d** which displayed significant elevation in the Bax / BCL-2 ratio was subjected to subsequent assessment of the levels of the effector caspase-7 and the initiator caspase-9. Treatment of MCF-7 cells with compound **9d** at its IC_{50} concentration 5.41 μM produced 4.44 folds increase in the level of the active effector caspase-7 and 10.99 folds elevation in the level of the initiator caspase-9 (Table 5).

3. Molecular modeling study

3.1. Molecular docking

In order to better understand the promising inhibitory activities of the newly synthesized compounds against VEGFR-2 kinase, molecular docking studies for the most potent compounds **7a**, **8c** and **9d** were performed. The docking studies were carried out within the active site of VEGFR-2 kinase. The binding site of VEGFR-2 kinase is characterized by front binding pocket which is ATP binding site marked by conserved traid (Aspartate-phenylalanine-Glycine, DFG motif)), and an additional hydrophobic back pocket which is allosteric binding pocket found in the inactive form of VEGFR-2 kinase [19]. According to the orientation of the DFG motif, the kinase adopted two conformations; the active conformation which is (DFG-in) conformation, and the inactive conformation which is (DFG-out); where the DFG motif adopted a closed conformation [19,52]. Generally, VEGFR-2 kinase inhibitors are classified into two main inhibitors groups according to their binding position; group I inhibitors, where the inhibitors bind to the ATP site in a similar manner to that of adenine. Group II inhibitors, where the inhibitors bind to ATP site and the auxiliary hydrophobic back pocket [19,20]. In general, group II inhibitors are more selective than group I. More recently, a new class of VEGFR-2 kinase inhibitors has been identified (group III inhibitors) which bind entirely beyond the gatekeeper residue to the allosteric site outside the ATP binding site adopting the inactive "DFG-out" conformation [21,22]. In this study we will investigate the binding mode of the three active compounds **7a**, **8c** and **9d** to identify the relationship between their activity and their interaction within VEGFR-2 kinase binding pocket.

Table 5
Caspases-7 & 9 concentrations in MCF-7 cells after treatment with compound **9d** for 24 h.

Compound	Conc (μM)	Casp7		Casp9	
		Conc. (ng/ml)	FLD	Conc. (ng/ml)	FLD
9d	5.41	1.597	4.44	17.91	10.99
Doxorubicin	6.73	1.9	5.29	25	15.34
Control	–	0.359	–	1.63	–

A close look to VEGFR-2 binding site showed that the key amino acids in the front pocket of the enzyme which contribute in H-bonds formation are Glu917 and Cys919, the two amino acids are located in the hinge region [53]. Some inhibitors formed H-bonds with Lys868. While the key amino acids in the hydrophobic back pocket are Glu885 and Asp1046 [53]. Furthermore, there is a hydrophobic region in the front pocket that included Leu840, Val848, Ala866, Lys868, Glu917, Phe918 and Gly922, while the hydrophobic part of the back pocket is formed of Ile888, Ile892, Val898, Val899, Leu1019, His1026, Ile1044, Cys1045 and Phe1047 [53–55]. The hydrophobic and Van Der Waals interactions play an important role in the binding affinity and selectivity of the inhibitors.

Docking study was carried out with MOE-2008 software [56] and the crystal structure (PDB: 3U6J) was used in our molecular study to explore new VEGFR-2 inhibitors [34]. Validation of the molecular docking protocol was done by re-docking the native ligand. Fig. 5 showed that the re-docked ligand has the same binding mode as the co-crystalized ligand. Besides, the RMSD value between the re-docked ligand and the co-crystalized one is too small (0.35 Å) and the binding score of the re-docked ligand is −10.54 Kcal/mol. The docking results of the re-docked ligand indicated the reliability of the docking protocol.

The re-docked ligand and the co-crystalized ligand showed the same orientation and the same interactions within the binding pocket residues. The co-crystalized ligand formed H-bonds with Lys868, Cys919 and Asp1046 (Fig. 5). The aromatic part of the quinoline group showed hydrophobic interactions with Leu840, Val848, Ala866, Leu868 and Phe918 (the front pocket) and the phenyl moiety of the native ligand illustrated hydrophobic interactions with Ile888, Ile892, Val898, Val899, Leu1019, His1026 and Leu1035 (the allosteric pocket). In addition, π-π interaction with Phe1047 was also observed (Table 6).

The binding mode of compound **7a** within VEGFR-2 binding site showed H-bonds with important residues of the front pocket. Thr916 which is one of the important amino acids in the front pocket formed two H-bonds with coumarin and pyrazole moieties. An extra H-bond between compound **7a** and Lys868 was observed. In total, compound **7a** formed three H-bonds with the key amino acids of the ATP binding site (front pocket) where the coumarin group acted as hydrogen bond acceptor (HBA) forming one H-bond with the side chain OH of Thr916. Similarly, the linker pyrazole moiety of compound **7a** participated in one H-bond where, the N atom at 2-position of the pyrazoline moiety acted as HBA and interacted with the OH of Thr916. The substituted thiazole group contributed by one H-bond *via* its N atom that acted as HBA and formed H-bond with side chain NH of Lys868 (Fig. 6). The aromatic part of coumarin ring interacted with the hydrophobic region within the front pocket through Leu840, Val848, Ala866 and Phe918.

In addition, π-π interaction between coumarin moiety and Phe1047 (one of the DFG motif) was recognized (Fig. 7). Despite the absence of H-bonds between compound **7a** and the key amino acids of the front pocket (Glu917 and Cys919), oxygen atom and carbonyl moiety of coumarin ring were in a close contact with these two amino acids which suggests hydrophilic interaction. On the other hand, the aromatic part of dimethylaminophenyl group interacted with Leu889, Ile892, Val898 and Val899 which are part of the hydrophobic back pocket (Fig. 7). It could be seen that, compound **7a** did not show H-bonds with the key

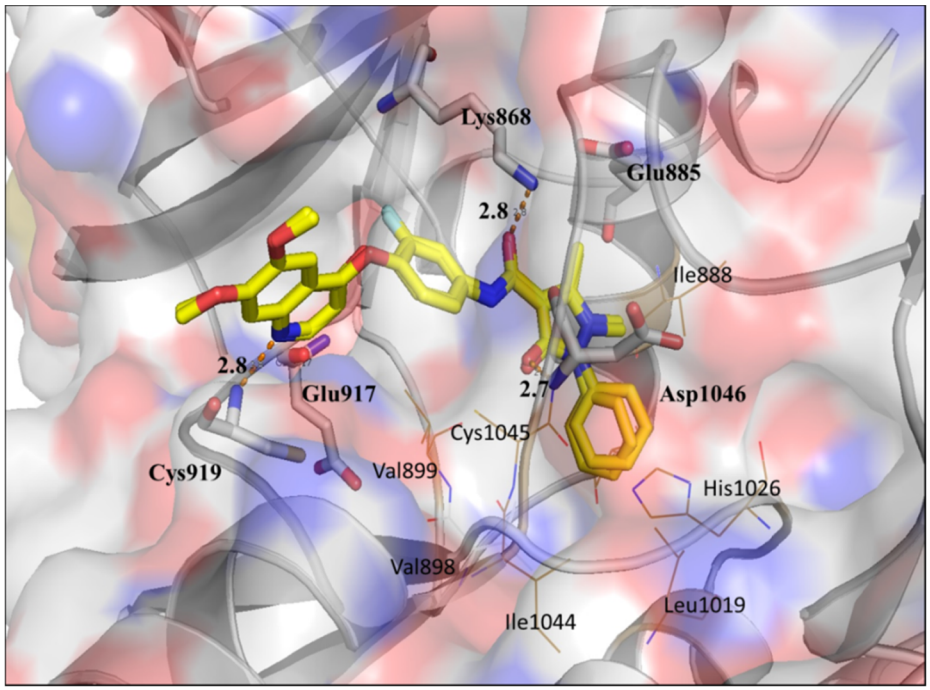

Fig. 5. Binding mode of the re-docked ligand within the binding pocket showed that it was superimposed on the same position as the native ligand (yellow, stick), showing the same orientation. The two ligands showed the same H-bonds profile with Lys868, Cys919 and Asp1046 (white, stick). The native ligand occupied the front pocket which is characterized by Glu917 and Cys919 and extend to the hydrophobic back pocket showing hydrophobic interactions with Ile888, Val898, Val899, Leu1019, His1026, Ile1044 and Cys1045 (brown, line). The binding pocket codes; C: pink, N: blue, H: white.

amino acids in the back binding pocket. However, the inhibitory activity of compound **7a** could be attributed to H-bond formation with important residues in the front pocket, besides the hydrophobic interactions with the front and the allosteric pocket which stabilize it within the binding site.

The inhibitory activity of compound **8c** is attributed to its biding mode which is different from that of compound **7a**. The introduction of ρ-chlorophenyldiazenyl substituent on the thiazole ring changed the orientation of compound **8c** within the active site of VEGFR-2 kinase. It was noticed that ρ-chlorophenyl moiety accommodated the front hydrophobic pocket and formed strong hydrophobic interactions with Leu840, Val848, Lys 868 and Phe918. Additionally, a close contact to the key amino acids Glu917 and Cys919 was also observed (Fig. 8). Furthermore, π-π interaction between ρ-chlorophenyl and Phe1047 which increased the binding interactions pattern was detected. The position of dimethylaminophenyl group allowed its hydrophobic interaction with the back hydrophobic pocket which was lined with the hydrophobic amino acids Leu886, Ile888, Leu889, Ile892, Val898, Val899, Leu1019 and His1026 maximizing the binding interactions with the pocket. Also, the hydrophilic part of coumarin moiety and the

Table 6
Docking results of compounds **7a, 8c, 9d** and the native ligand showing the main residues involved in the interactions and the docking score of the target compounds.

Comp no.	Moieties from the compound	Amino acid residues	Distance Å	Score Kcal/mol
Native ligand	C=O pyrazole	NH-Asp1046	2.7	−10.54
	C=O	NH-Lys868	2.8	
	N quinoline	NH-Cys919	2.8	
	Quinoline moiety	Hydrophobic interactions with Leu840, Val848, Ala866, Leu868 and Phe918		
	Phenyl group	Hydrophobic interactions with Ile888, Ile892, Val898, Val899, Leu1019, Leu1035 and His1026		
	Flourophenyl	π-π interaction with Phe1047		
7a	N thiazole	NH-Lys868	2.7	−8.82
	N pyrazole	OH Thr916	3.5	
	C=O coumarin	OH Thr916	2.7	
	Coumarin	Hydrophobic interactions with Leu840, Val848, Ala 866 and Phe918 π-π interaction with Phe1047		
	Dimethylaminophenyl	Hydrophobic interactions with Leu889, Ile892, Val898, Val899 and Leu889		
8c	N thiazole	NH-Lys868	3.3	−8.85
	p-Chlorophenyl	Hydrophobic interactions with Leu840, Val848, Lys 868, Phe 918. and close contact to the key amino acids Glu917 and Cys91 π-π interaction with Phe1047		
	Dimethylaminophenyl	Hydrophobic interactions with Leu886, Ile888, Leu889, Ile892, Val 898, Val899, Leu1019 and His1026		
9d	OH coumarin	C=O Asp1046	3.2	−11.10
		C=OGlu855	3.7	
	N pyrazole	NH Lys868	3.4	
	N thiazole	NH-Lys868	2.7	
	N diazine group	OH Thr916	3.7	
	p-Chlorophenyl and phenyl groups	Hydrophobic interactions with Leu840, Val 848, Ala866, Val848, Val898, Val899, Val914 and Phe918		
	Dimethylaminophenyl	Hydrophobic interactions with Leu886, Ile 888, Leu889, Ile892, Leu 1019, His 1026 and Ile1044		

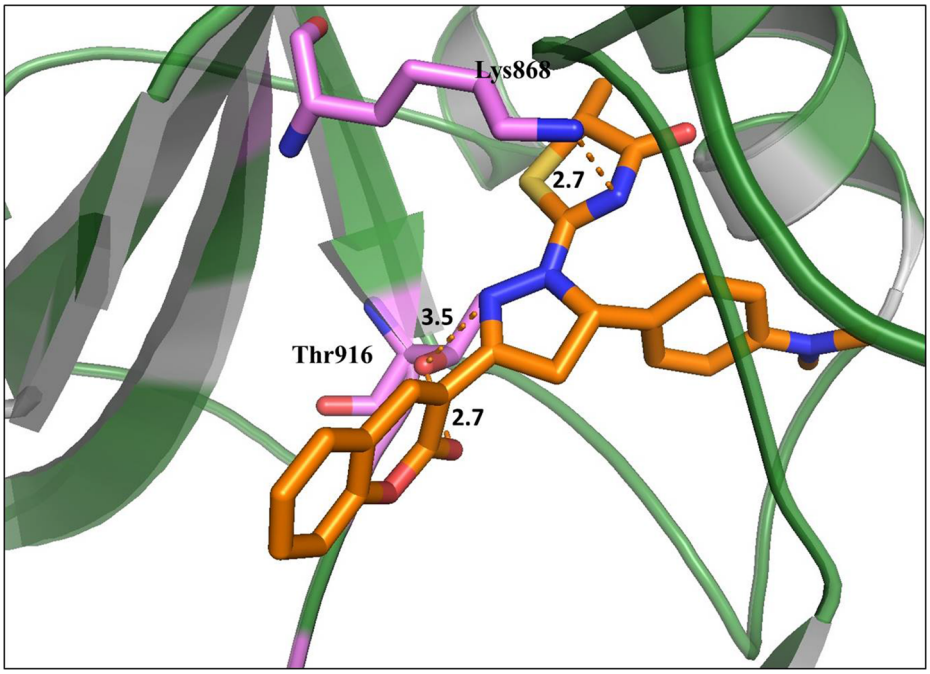

Fig. 6. Binding mode of compound **7a** (brown, stick), showed three H-bonds, OH Thr916 (pink, stick) formed two H-bonds with C═O coumarin, and N pyrazole. The third H-bond was between NH Lys868 (pink, stick) and thiazole. Protein is represented as green cartoon.

pyrazole group were in a close contact to Glu885 and Asp1046, the key residues of the back pocket. Moreover, N of thiazole ring of compound **8c** acted as HBA and formed one H-bond with NH Lys868 (3.3 Å) which is one of the key amino acids in ATP binding site (Fig. 8).

Compound **9d** illustrated the same orientation as compound **8c** that may be attributed to the presence of *p*-chlorophenyl moiety. In addition, the presence of an additional phenyl substituent on the thiazole group increased the hydrophobic interactions. Both *p*-chlorophenyl and phenyl groups showed hydrophobic interactions with Ala866, Leu840, Val848, Val898, Val899, Val914 and Phe918. The dimethylaminophenyl group showed the same hydrophobic interactions as that of compound **8c**, where it formed hydrophobic interactions with the allosteric hydrophobic pocket which included side chains of Leu886, Ile 888, Leu889, Ile892, Leu 1019, His 1026 and Ile1044 (Fig. 9). The hydrophobic interactions of the three moieties; *p*-chlorophenyl, phenyl and dimethylaminophenyl with the hydrophobic residues increased the binding pattern of compound **9d** which was explained in the superiority of its docking score (−11.10 Kcal/mol) compared to compound **8c** (−8.85 Kcal/mol). Moreover, compound **9d** was stabilized within the binding pocket by forming five H-bonds, two of these H-bonds were formed with the key residues of the back pocket, Glu855 and Asp1046 and OH of coumarin, which is not present in compounds **7a** and **8c**. The

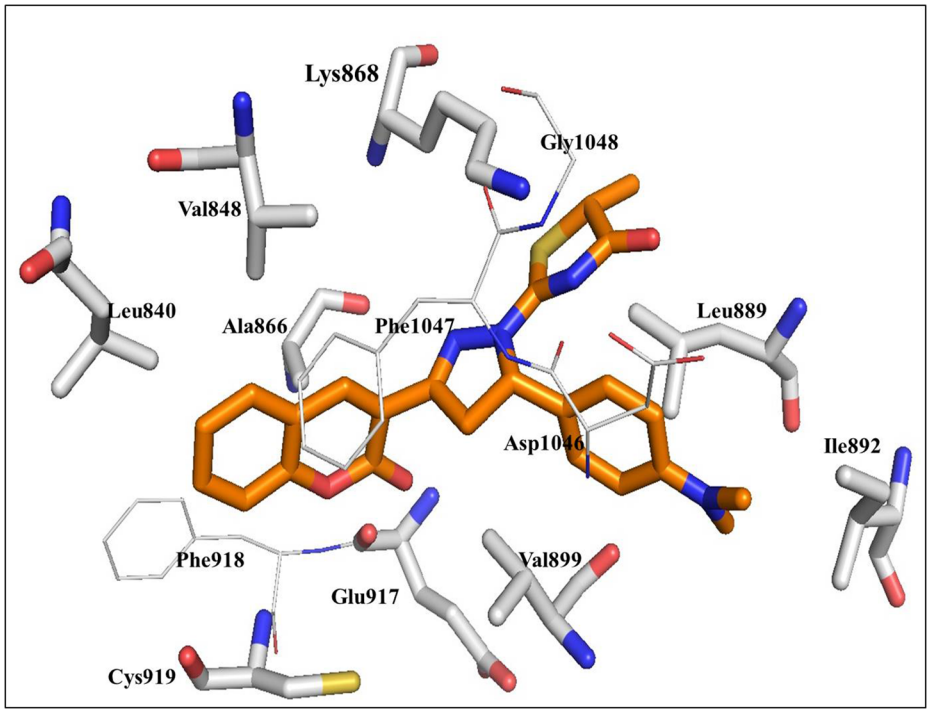

Fig. 7. Another view of compound **7a** (brown, stick) to illustrate its hydrophobic interactions, coumarin moiety showed hydrophobic interaction with Phe918, Leu840, Val848 and Ala866 (hydrophobic part of the front pocket). Dimethylaminophenyl moiety of compound **7a** showed hydrophobic interactions with some of the back pocket residues. All the residues are represented as (white, stick) expect the DFG motif and Phe918 which are represented as (while, line) for clarity.

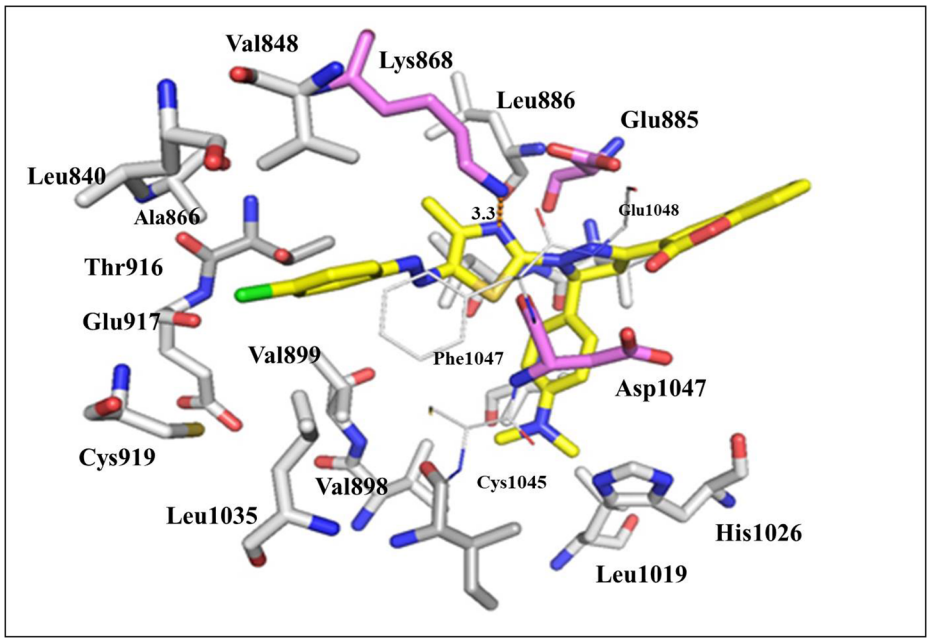

Fig. 8. Compound **8c** (yellow, stick) showed one H-bond between N thiazole and NH lys868 at a distance of 3.3 Å. *p*-Chlorophenyl group showed hydrophobic interactions with Leu840, Val848, and Lys 868,(front pocket), and a close contact to the key amino acids Glu917 and Cys919 was detected. Dimethylaminophenyl moiety showed hydrophobic interactions with Leu886, Val 898 and Val899. Coumarin and thiazole were in a close contact to Asp1046 and Glu885 (pink, stick).

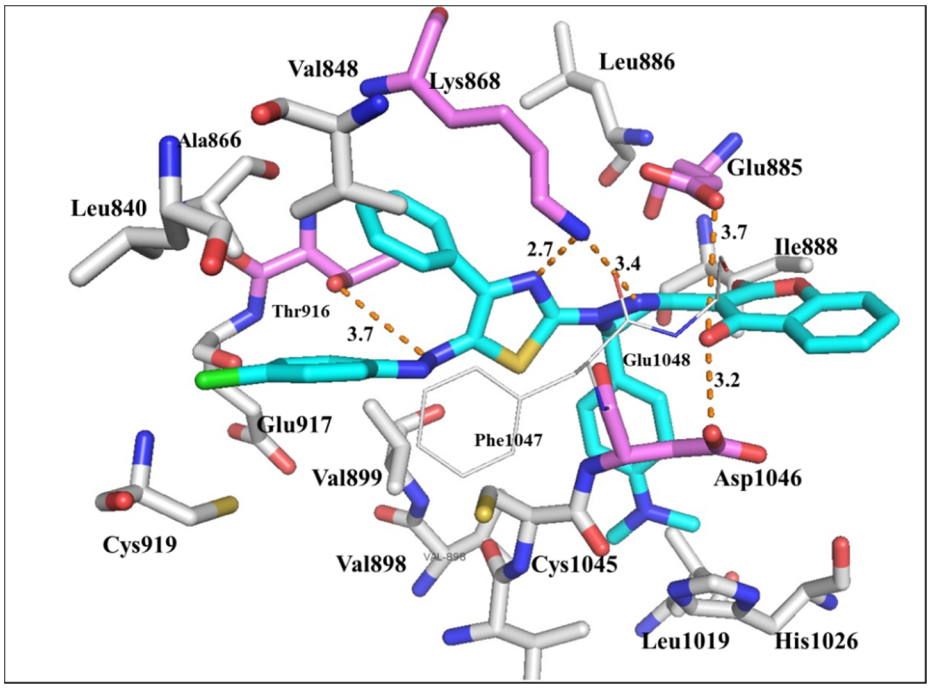

Fig. 9. Interactions of compound **9d** (cyan, stick), showed five H-bonds; OH coumarin formed two H-bonds with C═O Asp1046 and Glu885 (pink, stick). NH of Lys868 (pink, stick) formed two H-bonds with N of pyrazol and N of thiazol at distances of 3.4 Å and 2.7 Å respectively, and OH-Thr916 formed one H-bond with N of diazene at a distance of 3.7 Å. *p*-Chlorophenyl and phenyl groups showed hydrophobic interactions with Ala866, Leu840, Val848, Val898, Val899, Val914 and Phe918. Dimethylaminophenyl group formed hydrophobic interactions with the allosteric hydrophobic pocket which included side chains of Leu886, Ile 888, Leu889, Ile892, Leu 1019, His 1026 and Ile1044.

H-bond profile can be summarized as follows: OH coumarin acted as hydrogen bond donor (HBD) and formed two H-bonds one with C═O of Asp1046 and the other with C═O of Glu855. N of pyrazole and N of thiazole rings formed two H-bonds with NH Lys 868 at distances of 3.4 Å and 2.7 Å, respectively. Additionally, N of diazene group formed one H-bond with OH Thr916 at a distance of 3.7 Å (Fig. 9).

It was clear that the superiority of compound **9d** in the inhibitory activity against VEGFR-2 is related to its good binding mode through hydrophobic interactions with both ATP binding pocket and the allosteric site, in addition to its H-bonding profile where the presence of five H-bonds stabilized it within the two binding pockets, particularly the interaction of OH substituent of coumarin core with the two key residues of the hydrophobic back pocket (Glu855 and Asp1046).

The binding mode of the three inhibitors compared to the native ligand was illustrated in Fig. 10 where, the three compounds bound efficiently within the binding pocket. Compound **7a** occupied mainly the ATP binding pocket and as such considered as type I VEGFR-2 inhibitor, while both compounds **8c** and **9d** occupied ATP binding pocket and allosteric site and thus classified as type II inhibitors.

Although the three inhibitors did not form H-bonds with the key residues of the front pocket, (Glu917 and Cys919) they were in a close contact with them. Also, they formed H-bond with other front pocket residues as Thr916 and Lys868.

The superior activity of compounds **8c** and **9d** versus compound **7a** could be attributed to the presence of *p*-chlorophenyl group which forced the two compounds back within the allosteric site, consequently the coumarin moiety and the dimethyaminophenyl group were buried in the hydrophobic back pocket which facilitated good binding mode through hydrophobic interactions with the back pocket residues and also through H-bonds formation which improved their inhibitory

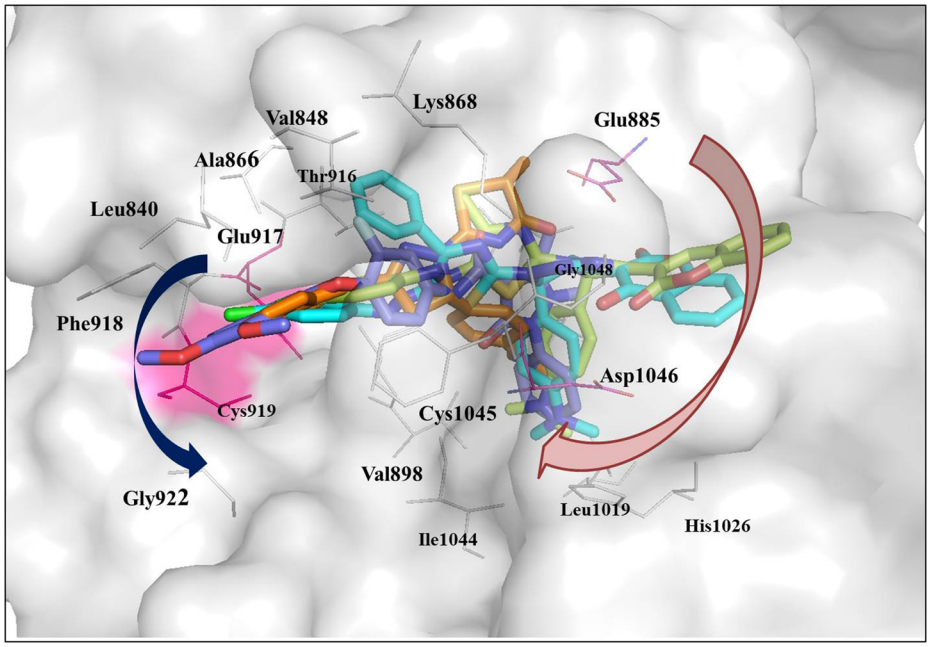

Fig. 10. binding mode of the native ligand (violet), compound **7a** (brown), compound **8c** (yellow) and compound **9d** (cyan). The three compounds had the same binding mode as the native ligand till a certain degree. The three compounds were in a close contact to the key residue (Glu917 and Cys919). Compound **7a** occupied ATP binding site. The presence of ρ-chlorophenyl group in compounds **8c** and **9d** changed their orientation. Both compounds moved back and the coumarin moiety was buried in the back binding pocket. The front pocket is represented by the blue arrow while the back pocket is represented by purple arrow.

activity. Furthermore, *p*-chlorophenyldiazenyl moiety in position 5 of thiazole ring increased the hydrophobic interactions with residues as Leu840, Val848, Al866, Lys 868 and Phe 918 (ATP binding pocket). The additional phenyl substituent in position 4 of thiazole ring in compound **9d** enhanced its orientation which was reflected in the high docking score (11.10 Kcal/mol).

3.2. Molecular dynamics studies (MD)

In the present study MD simulation was performed with GROMACS 5.1.2 software package. MD simulation takes the flexibility of protein and ligand into consideration which allows further evaluation of the reliability of docking results and also it can explore the residues in the active site and their interactions with the inhibitors during the simulation. In general, MD simulation creates ligand-receptor model state so close to the natural one, which gives a good opportunity to study the strength and continuity of the H-bonds profile.

The docked structures of the three promising inhibitors **7a**, **8c** and **9d** were used as initial structures for MD simulation. After completion of simulation process, the three complexes were checked for root mean square deviation (RMSD), root mean square fluctuation (RMSF), radius of gyration (Rg) and number of H-bonds formed between the inhibitors and the receptor.

Analysis of trajectories revealed that all the three systems in the simulation were well-equilibrated and remained stable throughout the simulation. The RMSD values of the backbone of the protein alone and the three inhibitor-protein complexes were calculated in order to investigate the stability of the complexes (Fig. 11). The final RMSD value of the three complexes and the protein remained below 0.2 nm during 10 ns simulation, which indicates that the protein structure is rigid in the presence of inhibitors during simulation. All the systems reached equilibrium at 1 ns except the protein which reached the platform at 6 ns. Compound **7a** which showed the least RMSD value 0.15 kept stabilized till the end of equilibrium. Both compounds **8c** and **9d** suddenly jumped to 0.2 nm at 4 ns which indicates slight conformational changes, as both compounds stabilized the protein in its two conformations DFG-in and DFG-out which is in agreement with our assumption from docking results.

The RMSF values of the residues in the inhibitors complexes and backbone protein alone were calculated to reveal the flexibility of VEGFR-2 backbone (Fig. 12). The high RMSF value indicates more

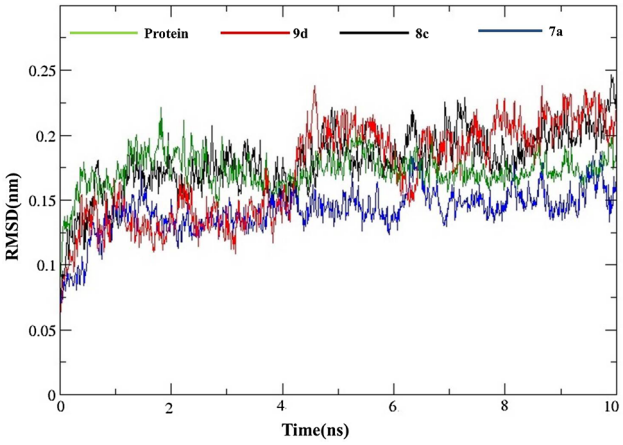

Fig. 11. RMSD of ligand-protein complexes during 10 ns MD simulations.

flexibility, while the low RMSF value indicates more stability during simulations. The results showed that the RMSF of the complexes is lower than that of the protein alone (Fig. 12A). RMSF plot of the binding pockets showed that regions Leu844-His878, Leu896-Phe921 and region Leu1035–Leu1049 were more stable than other regions, indicating that the residues in them were stabilized by interactions with the inhibitors (Fig. 12B). The first region included the conserved residues that form the hydrophobic part of the front pocket besides the key residue Lys868 which confirms our docking results where, the three inhibitors had hydrophobic interactions with the front pocket, besides the H-bond interaction with Lys868. Second and third regions included relatively conserved hydrogen interaction residues Glu917, Cys919 and Asp1046. These residues could form hydrogen bonds with the inhibitors and thus made these regions less flexible. It was clear that the three regions were highly rigid due to low RMSF value. The aforementioned findings were in accordance to molecular docking results where, compound **9d** formed H-bond with Asp1046 while compounds **7a** and **8c** were in a close contact to Glu917 and Cys919 which suggests the hydrophilic interactions with these key residues.

Also, the radius of gyration (Rg) for the three inhibitor-protein complexes and the backbone protein was calculated. Rg measures the distance of the region's parts from its centre of gravity. The radius of

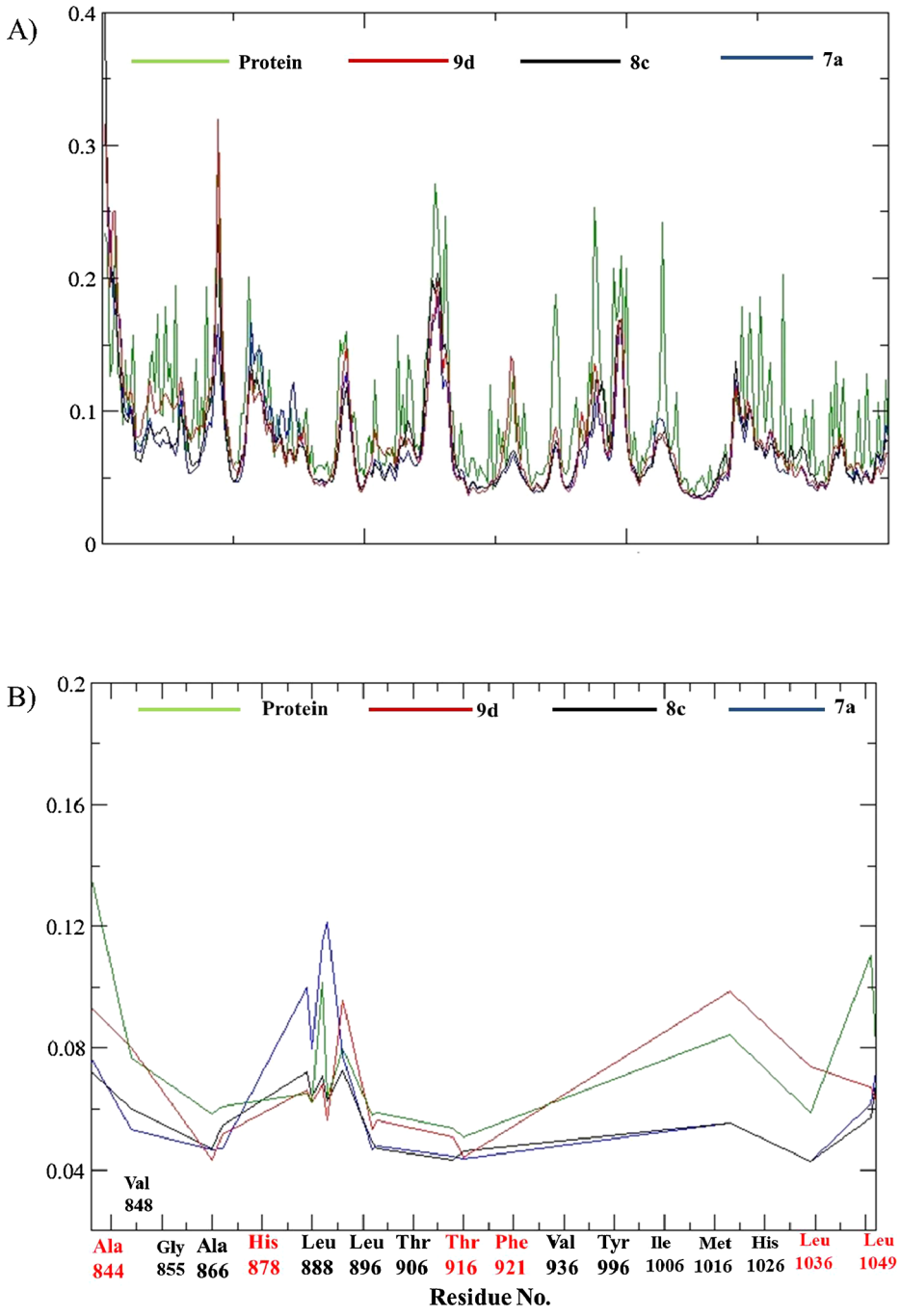

Fig. 12. (A) RMSF of ligand-protein complexes during 10 ns MD simulations. (B) RMSF of protein complex with the top three inhibitors and the binding site residues.

gyration of a protein is a measure of its compactness. If a protein is stably folded, it will maintain a relatively steady value of Rg and if a protein unfolds, its Rg will change over the time. The Rg of the three inhibitor-protein complexes remained steady over the dynamics and less than the protein alone which indicates the stability of the complexes of the ligands while the backbone protein is still dynamic during the simulation (Fig. 13).

Hydrogen bonds play an important role in stabilizing the protein-ligand complexes. As the ligands form more H-bonds with the protein, the protein-ligand complex becomes more stable. In the present study, hydrogen bond analysis was performed to depict the stability of the three inhibitor-protein complexes (Fig. 14). In case of compounds **7a** and **8c**, hydrogen bond interactions reached a maximum of four H-bonds and three of them remained for most of the time (Fig. 14A and B). Additionally, compound **9d** showed three H-bonds mainly with Asp1046 and Lys868 (Fig. 14C). The number of H-bonds of compound **7a** was in agreement with the docking results, while hydrogen bond analysis of compounds **8c** and **9d** were different from the docking results. MD of compound **8c** showed three stable H-bonds while docking studies showed only one, also, compound **9d** showed three H-bonds mainly with Asp1046 and Lys868, while docking results showed five H-bonds. There are no conflict between docking and MD results. As docking analysis assumes protein is rigid, so compounds may not be in the proper conformation to form H-bond, MD considers the flexibility of ligand and protein, so investigates all the conformations which may form H-bonds and also, it considers the stability of H-bond.

Consequently, the increase in the number of H-bonds of compound **8c** than that recognized from docking results, may be explained as,

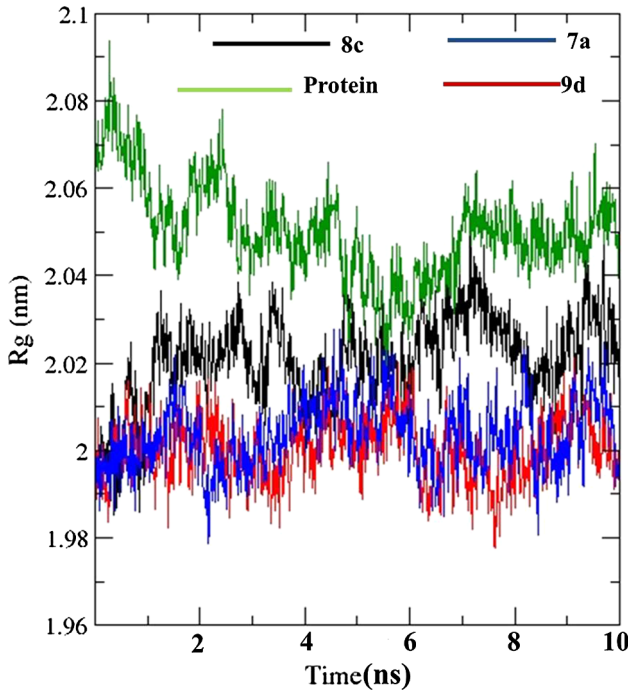

Fig. 13. Radius of gyration of the VEGFR-2 complex with the top three inhibitors.

according to docking analysis, compound **8c** was in a close contact to Glu 855 and Asp1046 but was not in a proper distance and angle to form H-bond, while during the simulation compound **8c** adopted different conformations in a proper distance and angle to form H-bonds with the residues.

However, in case of compound **9d**, the number of hydrogen bonding interactions reached up to three while the docking results revealed five H-bonds, this may be explained as two H-bonds had a distance of 3.7 Å which may not be stable enough during the simulation. Because compound **9d** is the most promising candidate, its H-bonds with Asp1046 (a key residue of allosteric pocket and DFG moiety) and Lys868 (one of the key residues of the front pocket) were investigated. Compound **9d** displayed one H-bond with Asp1046 which was strong and remained over the 10 ns (Fig. 14D), in addition, its interactions with Lys868 showed two H-bonds (Fig. 14E).

The H-bonds results indicate that the three inhibitors formed stable and strong H-bonds with the residues. Compound **9d** showed strong and stable H-bonds with Asp1046 and Lys868 (key residues).

3.3. QSAR study

QSAR analysis for the anti-proliferative activity of the synthesized compounds against MCF-7 cancer cells was performed in order to investigate the correlation between the physico-chemical parameters of the set of the synthesized compounds and their biological activity. The analysis was performed using MOE software. A set of the newly synthesized compounds was used as a training set with their measured pIC_{50} (the negative logarithmic value of the concentration required to produce 50% inhibition of the cancer cells). A wide range of 2D and 3D physicochemical descriptors of the training set were calculated and cross validation procedures were performed using leave one-out (LOO) cross-validation method, in which one compound is removed from the data set and the activity is calculated using the remaining of the data set. Squared correlation coefficient r^2, prediction r^2 (cross validation), standard error, root mean square error (RMSE) and residuals between the experimental and the predicted activity of the test set and the training set were used to validate QSAR models.

3.3.1. QSAR study result

The equation which represents the best QSAR model is:

$$-\log(IC_{50}) = 2.184 + 0.024\ \text{weight} - 0.033\ \text{E\_vdw} - 0.03120\ \text{vsurf\_D3} + 0.028\ \text{vsurf\_D5} - 0.404\ \text{Opr\_nrot}.$$

The experimental –log (IC_{50}) was plotted against the predicted –log (IC_{50}) (Fig. 15). Partial Least Squares method was used to build this model where, $r^2 = 0.85$, r^2 (pred) = 0.71 and REMS = 0.1.

According to the previous equation, the anti-proliferative activity of the newly synthesized compounds correlated positively with the weight and vsurf_D5 while it correlated negatively with E-vdw, vsurf_D3 and Opr_nrot.

Vsurf descriptors are volume and surface properties which depend on the structural connectivity and the conformation of the molecules [57]. These descriptors explain the interaction of molecules with the hydrophilic and hydrophobic part of the pocket site The vsurf_D descriptors explain the hydrophobic region of the molecules and are calculated at eight different energy levels (−0.2, −0.4, −0.6, −0.8, −1.0, −1.2, −1.4, and −1.6 kcal/mol) [57].

vsurf_D3 was calculated at −0.6 kcal/mol and its positive sign indicates the hydrophobic contribution of the molecules which is important for the activity, while vsurf_D5 was calculated at a different level of energy (−1.0 Kcal/mol) and its negative contribution illustrates that the presence of polar properties in the molecules could enhance their interactions with the active site. These results of the vsurf descriptors explained that the activity of the molecules was attributed to the balance between their hydrophobic and hydrophilic properties which was in agreement with the docking results, where, the biological activity requirements include hydrophobic interactions with the active site besides H-bond formation.

Also, Opr_nrot which is the number of rotatable bonds, correlated negatively with the −log (IC_{50}), which indicated that the decrease in the number of rotatable bonds is important for the activity.

3.3.2. QSAR validation

Reliability of the built QSAR model was verified using cross-validation; where r^2 (squared correlation coefficient value) equals 0.855 and r^2 (pred) is 0.71. In addition, the residuals between the experimental and the predicted activities of the training set were used to validate the established QSAR model (Table 7). It was found that the predicted values are close to those experimentally investigated, indicating that the QSAR model is reliable and can be safely applied for prediction of more effective compounds.

3.4. Bioavailability and drug likeness screening

Around fifteen highly predictive qualitative ADMET models were applied for calculating the physicochemical properties of the synthesized compounds, as blood brain barrier penetration, human intestinal absorption, cytochrome binding, biodegradation, acute oral toxicity, carcinogenicity, rat acute toxicity and aqueous solubility, using admetSAR server http://lmmd.ecust.edu.cn/admetsar1. It was found, that compounds **8c** and **9d** (Table 8) don not penetrate the blood brain barrier while compound **7a** was able to pass the blood brain barrier. All the compounds showed good intestinal absorption. Also, the compounds are found to be non-inhibitors of cytochrome (different profile were applied), which is one of important enzymes involved in drug metabolism. The three compounds showed good results against toxicity analysis. Besides, the candidate compounds illustrated good water solubility (Table 8). Moreover, molecular surface area of the three compounds were calculated, it is an important property to investigate the transport properties of the drug, as the polar surface area (PSA) is less than or equal to 140 Å, the compounds are considered orally active [57]. In our study the PSA of the three promising compounds is less

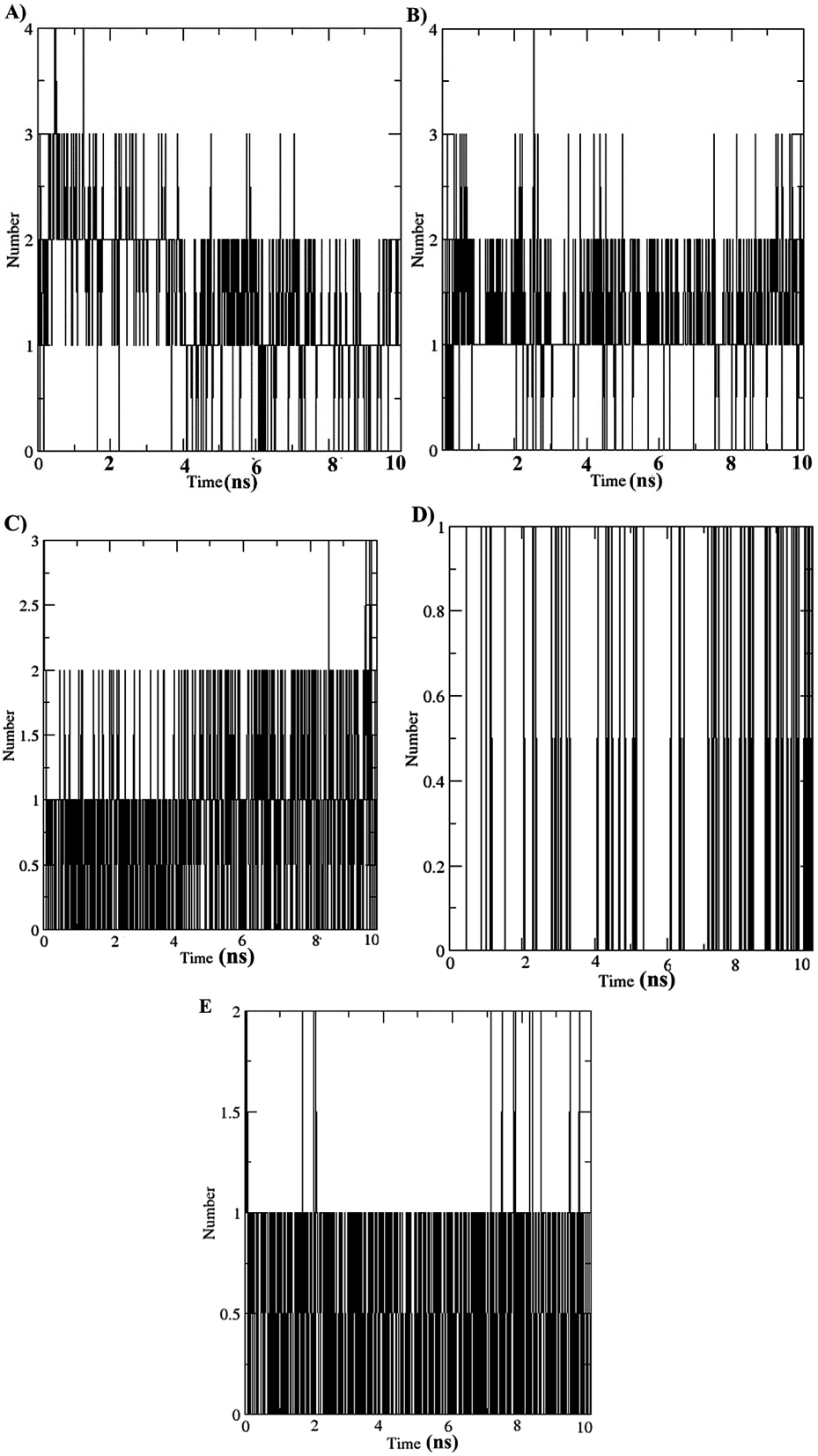

Fig. 14. H-bond formation of ligand-protein complexes as a function of time. (A) Compound **7a**. (B) Compound **8c**. (C) Compound **9d**. (D) H-bonds of compound **9d** with Asp1046. (E) H-bonds of compound **9d** with Lys868.

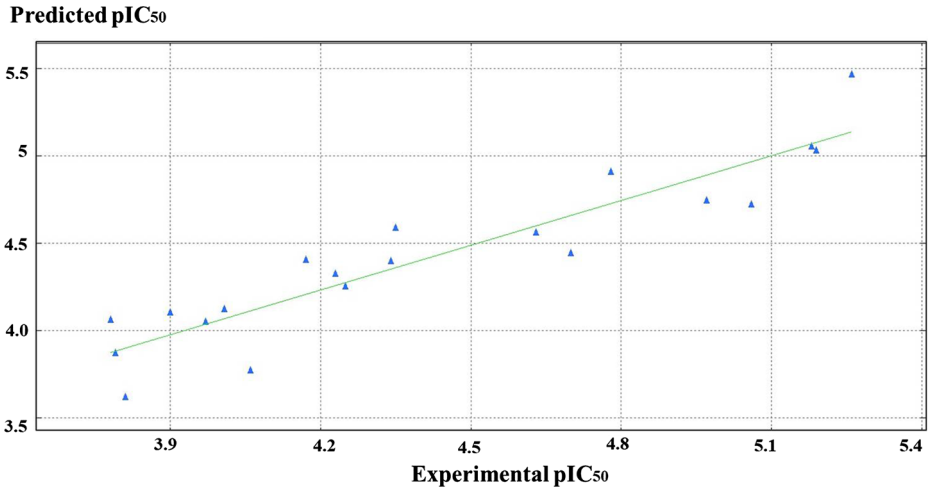

Fig. 15. Experimental versus predicted pIC_{50} of the tested compounds against MCF-7 human cancer cell line.

Table 7
The experimental and predicted pIC_{50} of the synthesized compounds.

Comp no.	Experimental pIC_{50}	Predicted pIC_{50}	Residual
2a	3.79	3.86	−0.07
2b	3.81	3.61	0.19
3a	3.78	4.05	−0.27
3b	4.06	3.76	0.29
4a	4.00	4.11	−0.11
4b	4.63	4.55	0.07
5a	4.23	4.32	−0.09
5b	4.70	4.44	0.25
6a	3.97	4.04	−0.07
6b	3.90	4.09	−0.19
7a	4.97	4.73	0.23
7b	4.17	4.40	−0.23
8a	4.25	4.24	0.01
8b	4.34	4.39	−0.05
8c	5.06	4.71	0.32
8d	4.78	4.90	−0.12
9a	4.35	4.58	−0.23
9b	5.18	5.04	0.13
9c	5.19	5.02	0.16
9d	5.2	5.46	−0.20

than 140 Å and the compounds are considered orally active. Overall, the excellent ADMET properties for the three compounds, except the positive result of blood brain barrier penetration of compound **7a**, make them promising candidates as anticancer agents.

4. Conclusion

In a summary, a new series of thiazolylpyrazolyl coumarin derivatives were designed and synthesized. The anticancer activity of the new compounds was evaluated *in vitro* against breast MCF-7, lung A549, prostate PC3 and liver HepG2 cancer cell lines in addition to normal melanocyte HFB4 cells. Five compounds **7a**, **8c**, **9b**, **9c** and **9d** displayed potent selective anticancer activity against MCF-7 with IC_{50} values ranging from 5.41 to 10.75 μM in comparison with the reference doxorubicin drug (IC_{50} = 6.73 μM). While three compounds **4b**, **5b** and **8d** showed moderate activity with IC_{50} values of 23.40, 19.96 and 15.53 μM, respectively. *In vitro* studies of VEGFR-2 inhibition in human breast cancer cells MCF-7 for the most promising cytotoxic compounds were consistent with their cytotoxic effects against MCF-7 showing that compounds **7a**, **8c**, **9b**, **9c** and **9d** were potent inhibitors at sub-micromolar concentrations when compared to the reference drug sorafenib (IC_{50} = 0.034–0.582 μM *vs* 0.019 μM for sorafenib) which suggests that the cytotoxic activities of target compounds could be referred

Table 8
Prediction of some of ADMET properties of hit compounds using admetSAR server.

Models	Compound **7a**	Compound **8c**	Compound **9d**
Blood-Brain Barrier	BBB +	BBB −	BBB −
Human Intestinal Absorption	HIA +	HIA +	HIA +
Renal Organic Cation Transporter	Non-inhibitor	Non-inhibitor	Non-inhibitor
CYP450 3A4 Substrate	Substrate	Substrate	Substrate
CYP450 1A2 Inhibitor	Non-inhibitor	Non-inhibitor	Non-inhibitor
CYP450 2D6 inhibitor	Non-inhibitor	Non-inhibitor	Non-inhibitor
CYP450 3A4 Inhibitor	Non-inhibitor	Non-inhibitor	Non-inhibitor
Human Ether-a-go-go-Related Gene Inhibition I	Weak inhibitor	Weak inhibitor	Weak inhibitor
Human Ether –a-go-go Related Gene Inhibition II	Non-inhibitor	Non-inhibitor	Non-inhibitor
AMES Toxicity	Non AMES toxic	Non AMES toxic	Non AMES toxic
Carcinogens	Non-carcinogens	Non-carcinogens	Non-carcinogens
Honey Bee Toxicity	Low HBT	Low HBT	Low HBT
Biodegradation	Not ready biodegradable	Not ready biodegradable	Not ready biodegradable
Acute Oral Toxicity	III	III	III
Carcinogenicity (three class)	Non-required	Non-required	Non-required
Rat Acute Toxicity (LD50, mol/kg)	2.4270	2.5688	2.5069
Aqueous solubility (Log s)	−3.4168	−3.852	−3.7144
PSA	74.5	82.7	102.9

to the inhibition of VEGFR-2. Activation of DNA damage response pathway for the most potent compound **9d** resulted in cell cycle arrest at G2/M phase, cell accumulation at pre-G1 phase and PI/ annexin-V staining. The mechanistic apoptosis pathway of compound **9d** was confirmed by the remarkable increase in the tumor suppressor gene p53 expression and elevation of Bax/Bcl-2 ratio, besides a significant increase in the levels of active caspases 7 and 9 was also detected which indicates the potent pro apoptotic efficiency of **9d** by inducing the intrinsic apoptotic pathway. Molecular docking was carried out for compounds **7a**, **8c** and **9d**. The three inhibitors showed good binding mode within the active pocket of VEGFR-2 enzyme, Compound **7a** occupied mainly the ATP binding site, while compounds **8c** and **9d** occupied the ATP binding pocket and the allosteric pocket. Hydrophobic interactions of the three compounds, characteristic π-π interactions with phe1047, one of DFG moieties, in addition to the different H-bonds profiles improve their binding and stabilization within the binding site. Molecular dynamics results illustrated deep information about interactions and stability of the three inhibitors within active binding pockets. The RMSD value of the three inhibitors reached equilibrium before the protein alone, which indicated that the three compounds stabilized the protein. RMSF results confirmed the stability of the kinase as a complex with the three inhibitors. QSAR model was built and the results showed that the $-\log IC_{50}$ correlated positively with the weight and vsurf_D5 while correlated negatively with E-vdw, vsurf_D3 and Opr_nrot. Different models were used to calculate the ADMET properties of the three active compounds, and the results indicated that these compounds are promising candidates as anticancer therapeutic agents.

5. Experimental

5.1. Chemistry

All melting points were uncorrected and measured using Electrothermal IA 9000 apparatus. Infrared spectra were measured by JASCO FT/IR-4100 spectrometer using KBr discs. The nuclear magnetic resonance NMR spectra were determined utilizing Varian mercury 300 MHz spectrometer and using TMS as the internal standard. The mass spectra were recorded on GCMS-QP 1000EX Shimadzu Gas Chromatography MS Spectrometer. IR, ^{1}H NMR, ^{13}C NMR, EI-MS and the elemental analyses were performed at Micro-Analytical Laboratory, Central Services Laboratory, Faculty of Science, Cairo University, Egypt. The reactions were followed by TLC (silica gel, aluminum sheets 60 F254, Merck) using chloroform-methanol (9.5:0.5 v/v) as eluent and sprayed with iodine-potassium iodide reagent. The purity of the newly synthesized compounds was assessed by TLC and elemental analysis and was found to be higher than 95%. Compounds **1a** [44] and **1b** [45] were previously prepared.

5.1.1. Preparation of 5-(4-(dimethylamino)phenyl)-4,5-dihydro-3-(4-(unsubstiuted/ hydroxy)-2-oxo-2H-chromen-3-yl)pyrazole-1-carbothioamides **2a,b**

A mixture of chalcones **1a,b** (0.01 mol), thiosemicarbazide (0.01 mol, 0.91gm) and a catalytic amount of HCl (1 mL) was refluxed in ethanol (30 mL) for 6–8 h. After cooling, the formed precipitate was filtered, washed with water, dried and recrystallized from acetic acid.

5.1.1.1. 5-(4-(Dimethylamino)phenyl)-4,5-dihydro-3-(2-oxo-2H-chromen-3-yl)pyrazole-1-carbothioamide ***2a***. Yield 80%, mp 254–6 °C. Anal. Calcd. for $C_{21}H_{20}N_4O_2S$ (392.47): C, 64.27; H, 5.14; N, 14.28; S, 8.17. Found: C, 64.49; H, 5.25; N, 14.39; S, 8.33. IR (cm^{-1}, KBr): 3398, 3219 (NH_2), 1725 (C═O), 1227 (C═S). ^{1}H NMR (DMSO-d_6, δ, ppm): 2.92 (6H, s, $N(CH_3)_2$), 3.29–3.35 (1H, dd, pyrazoline), 3.85–3.96 (1H, dd, pyrazoline), 5.88–5.93 (1H, dd, pyrazoline),7.06–8.50 (10*H*, m, Ar—H and NH_2), 8.73 (1H, s, H3-coumarin). MS (EI, 70 eV) *m/z* (%):392 (M^+) (72.49%), 146 (100.00%).

5.1.1.2. 5-(4-(Dimethylamino)phenyl)-4,5-dihydro-3-(4-hydroxy-2-oxo-2H-chromen-3-yl)pyrazole-1-carbothioamide ***2b***. Yield 83%, mp 226–8 °C. Anal. Calcd. for $C_{21}H_{20}N_4O_3S$ (408.47): C, 61.75; H, 4.94; N, 13.72; S, 7.85. Found: C, 62.01; H, 5.15; N, 13.91; S, 8.06. IR (cm^{-1}, KBr): 3423 (OH), 3297, 3174 (NH_2), 1700 (C═O), 1225 (C═S). ^{1}H NMR (DMSO-d_6, δ, ppm): 2.90 (6H, s, $N(CH_3)_2$), 3.29–3.41 (1H, dd, pyrazoline), 4.12–4.20 (1H, dd, pyrazoline), 5.28–5.41 (1H, dd, pyrazoline),7.06–8.50 (11*H*, m, Ar—H, OH and NH_2). MS (EI, 70 eV) *m/z* (%):408 (M^+) (9.15%), 121 (100.00%).

5.1.2. Preparation of 3-(5-(4-(dimethylamino)phenyl)-4,5-dihydro-1-(4-methyl/phenylthiazol-2-yl)-1H-pyrazol-3-yl)-4-(unsubstiuted/hydroxy)-2H-chromen-2-ones **3a,b, 4a,b** and ethyl 2-(5-(4-(dimethylamino)phenyl)-4,5-dihydro-3-(4-(unsubstiuted/hydroxy)-2-oxo-2H-chromen-3-yl) pyrazol-1-yl)-4-methylthiazole-5-carboxylates **5a,b**

A mixture of the thiocarbamoyl pyrazolines **2a,b** (0.001 mol) and the appropriate α-haloketones; chloroacetone, phenacyl bromide and/ or ethyl-2-chloroacetoacetate (0.001 mol) in ethanol (20 mL) in the presence of anhydrous sodium acetate (0.002 mol, 0.16gm) was refluxed for 6–8 h. After cooling, the formed precipitate was collected, washed with water, dried and recrystallized from acetic acid.

5.1.2.1. 3-(5-(4-(Dimethylamino)phenyl)-4,5-dihydro-1-(4-methylthiazol-2-yl)-1H-pyrazol-3-yl)-2H-chromen-2-one ***3a***. Yield 73%, mp 210–2 °C. Anal. Calcd. for $C_{24}H_{22}N_4O_2S$ (430.52): C, 66.96; H, 5.15; N, 13.01; S, 7.45. Found: C, 67.06; H, 5.29; N, 13.18; S, 7.65. IR (cm^{-1}, KBr): 1717 (C═O).^{1}H NMR (DMSO-d_6, δ, ppm): 2.08 (3H, s, CH_3), 2.86 (6H, s, N $(CH_3)_2$), 3.24–3.32 (1H, dd, pyrazoline), 3.94–4.04 (1H, dd, pyrazoline), 5.49–5.55 (1H, dd, pyrazoline), 6.44–7.89 (9H, m, Ar—H, and CH-thiazole), 8.47 (1H, s, H3-coumarin). MS (EI, 70 eV) *m/z* (%):430 (M^+) (46.54%), 121 (100.00%).

5.1.2.2. 3-(5-(4-(Dimethylamino)phenyl)-4,5-dihydro-1-(4-methylthiazol-2-yl)-1H-pyrazol-3-yl)-4-hydroxy-2H-chromen-2-one ***3b***. Yield 79%, mp > 300 °C. Anal. Calcd. for $C_{24}H_{22}N_4O_3S$ (446.52): C, 64.56; H, 4.97; N, 12.55; S, 7.18. Found: C, 64.76; H, 5.15; N, 12.72; S, 7.29. IR (cm^{-1}, KBr): 3423 (OH), 1716 (C═O). ^{1}H NMR ($CDCL_3$, δ, ppm): 2.21 (3H, s, CH_3), 2.96 (6H, s, $N(CH_3)_2$), 3.26–3.42 (1H, dd, pyrazoline), 4.19–4.29 (1H, dd, pyrazoline), 5.42–5.53 (1H, dd, pyrazoline), 6.44–8.47 (10*H*, m, Ar—H, CH-thiazole and OH). MS (EI, 70 eV) *m/z* (%):446 (M^+) (1.74%), 59 (100.00%).

5.1.2.3. 3-(5-(4-(Dimethylamino)phenyl)-4,5-dihydro-1-(4-phenylthiazol-2-yl)-1H-pyrazol-3-yl)-2H-chromen-2-one ***4a***. Yield 83%, mp 214–6 °C. Anal. Calcd. for $C_{29}H_{24}N_4O_2S$ (492.59): C, 70.71; H, 4.91; N, 11.37; S, 6.51. Found: C, 70.91; H, 5.05; N, 11.45; S, 6.70. IR (cm^{-1}, KBr): 1718 (C═O). ^{1}H NMR (DMSO-d_6, δ, ppm): 2.84 (6H, s, N $(CH_3)_2$), 3.39–3.46 (1H, dd, pyrazoline), 3.99–4.11 (1H, dd, pyrazoline), 5.58–5.64 (1H, dd, pyrazoline), 6.67–7.92 (14H, m, Ar—H and CH-thiazole), 8.59 (1H, s, H3-coumarin). MS (EI, 70 eV) *m/z* (%):492 (M^+) (51.08%), 121 (100.00%).

5.1.2.4. 3-(5-(4-(Dimethylamino)phenyl)-4,5-dihydro-1-(4-phenylthiazol-2-yl)-1H-pyrazol-3-yl)-4-hydroxy-2H-chromen-2-one ***4b***. Yield 85%, mp 148–50 °C. Anal. Calcd. for $C_{29}H_{24}N_4O_3S$ (508.59): C, 68.49; H, 4.76; N, 11.02; S, 6.30. Found: C, 68.65; H, 4.81; N, 11.12; S, 6.41. IR (cm^{-1}, KBr): 3426 (OH), 1718 (C═O). ^{1}H NMR (DMSO-d_6, δ, ppm): 2.89 (6H, s, N $(CH_3)_2$), 3.51–3.57 (1H, dd, pyrazoline), 4.13–4.23 (1H, dd, pyrazoline), 5.48–5.54 (1H, dd, pyrazoline), 6.78–8.03 (15H, m, Ar—H, CH-thiazole and OH). MS (EI, 70 eV) *m/z* (%):508 (M^+) (17.59%), 121 (100.00%).

5.1.2.5. Ethyl 2-(5-(4-(dimethylamino)phenyl)-4,5-dihydro-3-(2-oxo-2H-chromen-3-yl)pyrazol-1-yl)-4-methylthiazole-5-carboxylate ***5a***. Yield 87%, mp 236–8 °C. Anal. Calcd. for $C_{27}H_{26}N_4O_4S$ (502.58): C, 64.52; H, 5.21; N, 11.15; S, 6.38. Found: C, 64.70; H, 5.38; N, 11.25; S, 6.47.

IR (cm^{-1}, KBr): 1728 (C═O), 1673 (C═O). ^1H NMR ($CDCL_3$, δ, ppm): 1.31–1.36 (3H, t, $CH_2\underline{CH_3}$), 2.52 (3H, s, CH_3-thiazole), 2.94 (6H, s, N $(CH_3)_2$), 3.57–3.62 (1H, dd, pyrazoline), 4.02–4.15 (1H, dd, pyrazoline), 4.23–4.31(2H, q, $\underline{CH_2}CH_3$), 5.56–5.62 (1H, dd, pyrazoline), 6.65–7.64 (8H, m, Ar−H), 8.54 (1H, s, H3-coumarin). MS (EI, 70 eV) *m/z* (%):502 (M^+) (19.05%), 121 (100.00%).

5.1.2.6. Ethyl 2-(5-(4-(dimethylamino)phenyl)-4,5-dihydro-3-(4-hydroxy-2-oxo-2H-chromen-3-yl) pyrazol-1-yl)-4-methylthiazole-5-carboxylate ***5b***. Yield 82%, mp 230–2 °C. Anal. Calcd. for $C_{27}H_{26}N_4O_5S$ (518.58): C, 62.53; H, 5.05; N, 10.80; S, 6.18. Found: C, 62.71; H, 5.14; N, 10.92; S, 6.27. IR (cm^{-1}, KBr): 3432 (OH), 1727 (C═O), 1677 (C═O). ^1H NMR (DMSO-d_6, δ, ppm): 1.19–1.24 (3H, t, $CH_2\underline{CH_3}$), 2.42 (3H, s, CH_3-thiazole), 2.87 (6H, s, N $(CH_3)_2$), 3.53–3.59 (1H, dd, pyrazoline), 4.03–4.12 (1H, dd, pyrazoline), 4.13–4.17 (2H, q, $\underline{CH_2}CH_3$), 5.04–5.09 (1H, dd, pyrazoline), 6.67–7.92 (9H, m, Ar−H and OH). ^{13}C NMR (DMSO-d_6, δ ppm): 14.20, 17.14, 38.67, 49.04, 59.81, 61.09, 92.30, 108.21, 112.38, 115.57, 120.28, 121.91, 122.44, 125.20, 127.04, 131.43, 149.96, 153.04, 157.33, 158.91, 161.75, 162.69, 163.71, 174.02. MS (EI, 70 eV) *m/z* (%):518 (M^+) (12.84%), 121 (100.00%).

5.1.3. Preparation of 2-(5-(4-(dimethylamino)phenyl)-4,5-dihydro-3-(4-(unsubstiuted/hydroxy)-2-oxo-2H-chromen-3-yl)pyrazol-1-yl)-5-(unsubstiuted/methyl)-thiazol-4(5H)-ones ***6a,b*** *and* ***7a,b***

A mixture of the thiocarbamoyl pyrazolines **2a,b** (0.001 mol), ethylbromoacetate and/or ethyl 2-bromopropionate (0.001 mol) and anhydrous sodium acetate (0.002 mol,0.16gm) in ethanol (20 mL) was refluxed for 6-8 h. After cooling, the formed precipitate was collected, washed with water, dried and recrystallized from acetic acid.

5.1.3.1. 2-(5-(4-(Dimethylamino)phenyl)-4,5-dihydro-3-(2-oxo-2H-chromen-3-yl)pyrazol-1-yl)thiazol-4(5H)-one ***6a***. Yield 88%, mp 160–2 °C. Anal. Calcd. for $C_{23}H_{20}N_4O_3S$ (432.49): C, 63.87; H, 4.66; N, 12.95; S, 7.41. Found: C, 64.02; H, 4.84; N, 13.13; S, 7.57. IR (cm^{-1}, KBr): 1677 (C═O), 1609 (C═O). ^1H NMR (DMSO-d_6, δ, ppm): 2.86 (6H, s, N $(CH_3)_2$), 3.40–3.46 (1H, dd, pyrazoline), 3.92 (2H, s, CH_2-thiazolidinone), 4.03–4.13 (1H, dd, pyrazoline), 5.63–5.67 (1H, dd, pyrazoline), 6.66–7.94 (8H, m, Ar−H), 8.64 (1H, s, H3-coumarin). ^{13}C NMR (DMSO-d_6, δ ppm): 38.67, 44.79, 63.28, 112.23, 115.98, 118.04, 118.40, 124.81, 126.63, 127.38, 129.63, 133.44, 143.35, 149.98, 153.64, 157.03, 157.40, 160.76, 186.77. MS (EI, 70 eV) *m/z* (%):432 (M^+) (59.56%), 261 (100.00%).

5.1.3.2. 2-(5-(4-(Dimethylamino)phenyl)-4,5-dihydro-3-(4-hydroxy-2-oxo-2H-chromen-3-yl)pyrazol-1-yl)thiazol-4(5H)-one ***6b***. Yield 87%, mp > 300 °C. Anal. Calcd. for $C_{23}H_{20}N_4O_4S$ (448.49): C, 61.59; H, 4.49; N, 12.49; S, 7.15. Found: C, 61.72; H, 4.63; N, 12.64; S, 7.25. IR (cm^{-1}, KBr): 3425 (OH), 1675 (C═O), 1607 (C═O). ^1H NMR (DMSO-d_6, δ, ppm): 2.85 (6H, s, N $(CH_3)_2$), 3.60–3.64 (1H, dd, pyrazoline), 3.75 (2H, s, CH_2-thiazolidinone), 3.89–3.99 (1H, dd, pyrazoline), 5.34–5.38 (1H, dd, pyrazoline), 6.65–7.93 (9H, m, Ar−H and OH). MS (EI, 70 eV) *m/z* (%): 448 (M^+) (0.22%), 55 (100.00%).

5.1.3.3. 2-(5-(4-(Dimethylamino)phenyl)-4,5-dihydro-3-(2-oxo-2H-chromen-3-yl)pyrazol-1-yl)-5-methylthiazol-4(5H)-one ***7a***. Yield 84%, mp 236–8 °C. Anal. Calcd. for $C_{24}H_{22}N_4O_3S$ (446.52): C, 64.56; H, 4.97; N, 12.55; S, 7.18. Found: C, 64.72; H, 5.12; N, 12.71; S, 7.28. IR (cm^{-1}, KBr): 1729 (C═O), 1608 (C═O). ^1H NMR (DMSO-d_6, δ, ppm): 1.44–1.49 (3H, dd, CH_3), 2.85 (6H, s, N $(CH_3)_2$), 3.41–3.43 (1H, dd, pyrazoline), 4.07–4.14 (1H, dd, pyrazoline), 4.15–4.19 (1H, q, CH-thiazolidinone), 5.64–5.68 (1H, dd, pyrazoline), 6.67–7.93 (8H, m, Ar−H), 8.63 (1H, s, H3-coumarin). ^{13}C NMR (DMSO-d_6, δ ppm): 18.51, 38.67, 44.82, 48.63, 63.18, 112.23, 115.98, 118.40, 125.17, 126.67, 127.42, 129.00, 129.61, 133.44, 143.35, 149.94, 153.64, 157.07, 157.37, 176.02, 189.48. MS (EI, 70 eV) *m/z* (%):446 (M^+) (64.43%), 275 (100.00%).

5.1.3.4. 2-(5-(4-(Dimethylamino)phenyl)-4,5-dihydro-3-(4-hydroxy-2-oxo-2H-chromen-3-yl)pyrazol-1-yl)-5-methylthiazol-4(5H)-one ***7b***. Yield 85%, mp > 300 °C. Anal. Calcd. for $C_{24}H_{22}N_4O_4S$ (462.52): C, 62.32; H, 4.79; N, 12.11; S, 6.93. Found: C, 62.51; H, 4.91; N, 12.21; S, 7.07. IR (cm^{-1}, KBr): 3423 (OH), 1727 (C═O), 1607 (C═O). ^1H NMR (DMSO-d_6, δ, ppm): 1.41–1.48 (3H, dd, CH_3), 2.87 (6H, s, N $(CH_3)_2$), 3.58–3.66 (1H, dd, pyrazoline), 3.93–4.01(1H, dd, pyrazoline), 4.11–4.16 (1H, q, CH-thiazolidinone), 5.34–5.38 (1H, dd, pyrazoline), 6.65–7.93 (9H, m, Ar−H and OH). MS (EI, 70 eV) *m/z* (%): 463 ($M^+ + 1$) (0.24%), 59 (100.00%).

5.1.4. Preparation of 3-(5-(4-(Dimethylamino)phenyl)-4,5-dihydro-1-(4-methyl-5-(4-tolyl/ 4-chloro phenyldiazenyl)thiazol-2-yl)-1H-pyrazol-3-yl)-4-(unsubstiuted/hydroxy)-2H-chromen-2-ones ***8a-d***

A mixture of the thiocarbamoyl pyrazolines **2a,b** (0.001 mol) and the appropriate hydrazonoyl chlorides (0.001 mol) in dioxane (20 mL) containing a catalytic amount of triethylamine was refluxed for 5–7 h. After cooling, the formed precipitate was filtered, washed with water, dried and recrystallized from dioxane to give compounds **8a–d**.

5.1.4.1. 3-(5-(4-(Dimethylamino)phenyl)-4,5-dihydro-1-(4-methyl-5-(4-tolyldiazenyl)thiazol-2-yl)-1H-pyrazol-3-yl)-2H-chromen-2-one ***8a***. Yield 77%, mp 278–80 °C. Anal. Calcd. for $C_{31}H_{28}N_6O_2S$ (548.66): C, 67.86; H, 5.14; N, 15.32; S, 5.84. Found: C, 68.01; H, 5.24; N, 15.50; S, 5.97. IR (cm^{-1}, KBr): 1663 (C═O), 1528 (N═N). ^1H NMR (DMSO-d_6, δ, ppm): 2.36 (3H, s, CH_3), 2.51 (3H, s, CH_3), 2.87 (6H, s, N $(CH_3)_2$), 3.39–3.46 (1H, dd, pyrazoline), 4.02–4.09 (1H, dd, pyrazoline), 5.71–5.76 (1H, dd, pyrazoline), 6.68–7.94 (12H, m, Ar−H), 8.65 (1H, s, H3-coumarin). MS (EI, 70 eV) *m/z* (%): 548 (M^+) (100.00%).

5.1.4.2. 3-(5-(4-(Dimethylamino)phenyl)-4,5-dihydro-1-(4-methyl-5-(4-tolyldiazenyl)thiazol-2-yl)-1H-pyrazol-3-yl)-4-hydroxy-2H-chromen-2-one ***8b***. Yield 75%, mp 295–7 °C. Anal. Calcd. for $C_{31}H_{28}N_6O_3S$ (564.66): C, 65.94; H, 5.00; N, 14.88; S, 5.68. Found: C, 66.10; H, 5.13; N, 15.02; S, 5.85. IR (cm^{-1}, KBr): 3433 (OH), 1653 (C═O), 1519 (N═N). ^1H NMR (DMSO-d_6, δ, ppm): 2.33 (3H, s, CH_3), 2.51 (3H, s, CH_3), 2.86 (6H, s, N $(CH_3)_2$), 3.61–3.67 (1H, dd, pyrazoline), 4.30–4.34(1H, dd, pyrazoline), 5.26–5.35 (1H, dd, pyrazoline), 6.68–7.95 (13H, m, Ar − H and OH). MS (EI, 70 eV) *m/z* (%):564 (M^+) (0.44%), 57(100.00%).

5.1.4.3. 3-(5-(4-(Dimethylamino)phenyl)-4,5-dihydro-1-(4-methyl-5-(4-chlorophenyldiazenyl)thiazol-2-yl)-1H-pyrazol-3-yl)-2H-chromen-2-one ***8c***. Yield 76%, mp 104–6 °C. Anal. Calcd. for $C_{30}H_{25}ClN_6O_2S$ (569.08): C, 63.32; H, 4.43; N, 14.77; S, 5.63. Found: C, 63.50; H, 4.59; N, 14.91; S, 5.73. IR (cm^{-1}, KBr): 1670 (C═O), 1522 (N═N). ^1H NMR (DMSO-d_6, δ, ppm): 2.52 (3H, s, CH_3), 2.87 (6H, s, N $(CH_3)_2$), 3.40–3.47 (1H, dd, pyrazoline), 4.03–4.12 (1H, dd, pyrazoline), 5.71–5.75 (1H, dd, pyrazoline), 7.11–7.93 (12H, m, Ar−H), 8.64 (1H, s, H3-coumarin). MS (EI, 70 eV) *m/z* (%): 569, 571 (M^+, $M^+ + 2$) (22.80, 8.45%), 121 (100.00%).

5.1.4.4. 3-(5-(4-(Dimethylamino)phenyl)-4,5-dihydro-1-(4-methyl-5-(4-chlorophenyldiazenyl)thiazol-2-yl)-1H-pyrazol-3-yl)-4-hydroxy-2H-chromen-2-one ***8d***. Yield 77%, mp 126–8 °C. Anal. Calcd. for $C_{30}H_{25}ClN_6O_3S$ (585.08): C, 61.59; H, 4.31; N, 14.36; S, 5.48. Found: C, 61.70; H, 4.44; N, 14.51; S, 5.59. IR (cm^{-1}, KBr): 3433 (OH), 1672 (C═O), 1523 (N═N). ^1H NMR (DMSO-d_6, δ, ppm): 2.51 (3H, s, CH_3), 2.88 (6H, s, N $(CH_3)_2$), 3.39–3.43 (1H, dd, pyrazoline), 4.12–4.22 (1H, dd, pyrazoline), 5.26–5.39 (1H, dd, pyrazoline), 6.72–8.01 (13H, m, Ar − H). MS (EI, 70 eV) *m/z* (%):585, 587 (M^+, $M^+ + 2$) (0.26, 0.08%), 121 (100.00%).

5.1.5. Preparation of 3-(5-(4-(Dimethylamino)phenyl)-4,5-dihydro-1-(4-phenyl-5-(4-tolyl/4-chlorophenyldiazenyl)thiazol-2-yl)-1H-pyrazol-3-yl)-4-(unsubstiuted/hydroxy)-2H-chromen-2-ones ***9a-d***

To a solution of **4a,b** (0.001 mol) in ethanol (20 mL), sodium

acetate trihydrate (0.001 mol, 0.14 g) was added and the mixture was cooled to 0–5 °C in an ice bath. To the resulting cold solution, a cold solution of arenediazonium chloride [prepared by diazotizing aniline derivatives (0.001 mol) dissolved in hydrochloric acid (6 M, 1 mL) with a solution of sodium nitrite (0.001 mol, 0.07 gm) in water (2 mL)], was added portionwise. After complete addition of the diazonium salt, the reaction mixture was stirred for 30 min in an ice bath. The solid that separated out was filtered off, washed with water and recrystallized from ethanol to give the title compounds **9a-d**.

5.1.5.1. 3-(5-(4-(Dimethylamino)phenyl)-4,5-dihydro-1-(4-phenyl-5-(4-tolyldiazenyl)thiazol-2-yl)-1H-pyrazol-3-yl)-2H-chromen-2-one ***9a***. Yield 82%, mp 242–4 °C. Anal. Calcd. for $C_{36}H_{30}N_6O_2S$ (610.73): C, 70.80; H, 4.95; N, 13.76; S, 5.25. Found: C, 70.92; H, 5.06; N, 13.89; S, 5.37. IR (cm^{-1}, KBr): 1717 (C═O), 1521 (N═N). ^1H NMR (DMSO-d_6, δ, ppm): 2.40 (3H, s, CH_3), 2.85 (6H, s, N $(CH_3)_2$), 3.36–3.44 (1H, dd, pyrazoline), 4.00–4.10 (1H, dd, pyrazoline), 5.59–5.62 (1H, dd, pyrazoline), 6.67–7.89 (17H, m, Ar—H), 8.52 (1H, s, H3-coumarin). MS (EI, 70 eV) *m/z* (%):610 (M^+) (100.00%).

5.1.5.2. 3-(5-(4-(Dimethylamino)phenyl)-4,5-dihydro-1-(4-phenyl-5-(4-tolyldiazenyl)thiazol-2-yl)-1H-pyrazol-3-yl)-4-hydroxy-2H-chromen-2-one ***9b***. Yield 79%, mp 156–8 °C. Anal. Calcd. for $C_{36}H_{30}N_6O_3S$ (626.73): C, 68.99; H, 4.82; N, 13.41; S, 5.12. Found: C, 69.12; H, 4.94; N, 13.58; S, 5.22. IR (cm^{-1}, KBr): 3431 (OH), 1717 (C═O), 1521 (N═N). ^1H NMR ($CDCL_3$, δ, ppm): 2.41 (3H, s, CH_3), 2.99 (6H, s, N $(CH_3)_2$), 3.85–3.94 (1H, dd, pyrazoline), 4.21–4.28 (1H, dd, pyrazoline), 5.65–5.672 (1H, dd, pyrazoline), 7.24–8.24 (18H, m, Ar—H and OH). MS (EI, 70 eV) *m/z* (%): 626 (M^+) (0.86%), 107 (100.00%).

5.1.5.3. 3-(5-(4-(Dimethylamino)phenyl)-4,5-dihydro-1-(4-phenyl-5-(4-chlorophenyldiazenyl)thiazol-2-yl)-1H-pyrazol-3-yl)-2H-chromen-2-one ***9c***. Yield 80%, mp 174–6 °C. Anal. Calcd. for $C_{35}H_{27}ClN_6O_2S$ (631.15): C, 66.60; H, 4.31; N, 13.32; S, 5.08. Found: C, 66.71; H, 4.48; N, 13.45; S, 5.19. IR (cm^{-1}, KBr): 1715 (C═O), 1517 (N═N). ^1H NMR (DMSO-d_6, δ, ppm): 2.89 (6H, s, N $(CH_3)_2$), 3.49–3.56 (1H, dd, pyrazoline), 4.00–4.18 (1H, dd, pyrazoline), 5.75–5.82 (1H, dd, pyrazoline), 6.90–8.15 (17H, m, Ar—H), 8.62 (1H, s, H3-coumarin). ^{13}C NMR (DMSO-d_6, δ ppm): 43.24, 44.68, 63.01, 116.04, 117.23, 118.33, 118.55, 119.05, 120.42, 123.42, 124.90, 127.49, 127.61, 128.46, 129.46, 129.86, 131.53, 133.19, 133.38, 133.65, 142.23, 143.61, 150.96, 153.22, 153.57, 157.75, 158.57. MS (EI, 70 eV) *m/z* (%): 631, 633 (M^+, $M^+ + 2$) (31.24, 10.12%), 121 (100.00%).

5.1.5.4. 3-(5-(4-(Dimethylamino)phenyl)-4,5-dihydro-1-(4-phenyl-5-(4-chlorophenyldiazenyl)thiazol-2-yl)-1H-pyrazol-3-yl)-4-hydroxy-2H-chromen-2-one ***9d***. Yield 81%, mp 148–50 °C. Anal. Calcd. for $C_{35}H_{27}ClN_6O_3S$ (647.15): C, 64.96; H, 4.21; N, 12.99; S, 4.95. Found: C, 65.06; H, 4.35; N, 13.12; S, 5.09. IR (cm^{-1}, KBr): 3430 (OH), 1715 (C═O), 1518 (N═N). ^1H NMR (DMSO-d_6, δ, ppm): 2.86 (6H, s, N $(CH_3)_2$), 3.57–3.64 (1H, dd, pyrazoline), 4.07–4.18 (1H, dd, pyrazoline), 5.57–5.60 (1H, dd, pyrazoline), 6.69–8.17 (18H, m, Ar—H and OH). MS (EI, 70 eV) *m/z* (%):647, 649 (M^+, $M^+ + 2$) (1.37, 0.42%), 121 (100.00%).

5.2. Biology

5.2.1. Anticancer assessment

5.2.1.1. Chemicals and cell culturing. Fetal bovine serum (FBS) and L-glutamine, were obtained from Gibco Invitrogen Company (Scotland, UK). Dulbecco's modified Eagle's medium (DMEM) was provided from Cambrex (New Jersey, USA). Dimethylsulfoxide (DMSO), doxorubicin, penicillin, streptomycin and Sulfo-Rhodamine-B stain (SRB) (3-(4,5-dimethylthiazol-2-yl)-2,5-diphenyltetrazolium bromide) were obtained from Sigma-Aldrich (St. Louis, MO, USA). All other chemicals and reagents used in this study were of analytical grade and were purchased from Sigma-Aldrich (St. Louis, MO, USA). Human Vascular Endothelial Growth Factor (VEGFR-2) ELISA kit was purchased from Boster Biological Technology Co., Ltd (3942 B Valley Ave, Pleasanton, CA, 94566, USA). The lung A549, breast MCF-7, prostate PC3 and liver HepG2 cancer cell lines as well as the normal cell line (human normal melanocyte, HFB4) were obtained from the American Type Culture Collection (Rockville, MD, USA). Cells were maintained in Dulbecco's modified Eagle's medium (DMEM) and supplemented with 10% heat inactivated fetal calf serum (GIBCO), penicillin (100 U/ml) and streptomycin (100 µg/mL) at 37 °C in humidified atmosphere containing 5% CO_2. Cells at a concentration of 0.50×10^4 were grown in a 25 cm^3 flask in 5 mL of culture medium.

5.2.1.2. Anticancer activity assay. The anticancer activity of the synthesized compounds **2–9** was measured *in vitro* using the Sulfo-Rhodamine-B stain (SRB) assay according to Skehan et al. [58] and modified by Ali et al. [59]. Briefly, cells were inoculated in 96-well microtiter plate (104 cells/well) for 24 h before treatment with the tested compounds to allow attachment of cells to the wall of the plate. Test compounds were dissolved in DMSO at 1 mg/mL immediately before use and diluted to the appropriate volume just before addition to the cell culture. Different concentration of tested compounds and doxorubicin were added to the cells. Three wells were prepared for each individual dose. Monolayer cells were incubated with the compounds for 48 h at 37 °C and in an atmosphere of 5% CO_2. After 48 h, cells were fixed, washed, and stained for 30 min with 0.4% (w/v) SRB dissolved in 1% acetic acid. Unbound dye was removed by four washes with 1% acetic acid, and the attached stain was recovered with Tris-EDTA buffer. Color intensity was measured in an ELISA reader. The relation between surviving fraction and drug concentration is plotted to get the survival curve for each cell line after the specified time. The concentration required for 50% inhibition of cell viability (IC_{50}) was calculated and the results are given in Table 1. The results were compared to the effect of doxorubicin as a reference drug.

5.2.2. In vitro VEGFR-2 inhibition assays

5.2.2.1. In vitro effect of the synthesized compounds on the level of VEGFR-2 in MCF-7 cells. The effect of the most promising cytotoxic compounds **4b**, **5b**, **7a**, **8c**, **8d**, **9b**, **9c** and **9d** on the level of VEGFR-2 in human breast cancer cell line MCF-7 was determined. The cells in culture medium were treated with 20 µL of IC_{50} values of the compounds dissolved in DMSO, then incubated for 24 h at 37 °C, in a humidified 5% CO_2 atmosphere. The cells were harvested and the homogenates were prepared in saline using a tight pestle homogenizer until complete cell disruption. The kit uses a double-antibody sandwich enzyme-linked immunosorbent assay (ELISA) to determine the level of human VEGFR-2 in samples. A monoclonal antibody for VEGFR-2 was pre-coated onto 96-well plates. The test samples are added to the wells and a biotinylated detection polyclonal antibody from goat specific for VEGFR-2 was added subsequently followed by washing with PBS buffer. Avidin-Biotin-Peroxidase complex was added and the unbound conjugates were washed away with PBS buffer. HRP substrate, TMB, was used to visualize HRP enzymatic reaction. TMB was catalyzed by HRP to produce a blue color product that changed into yellow after adding acidic stop solution. The density of yellow color is proportional to the human VEGFR-2 amount of the sample captured in the plate. The chroma of color and the concentration of the human VEGFR-2 of the samples were positively correlated and the optical density was determined at 450 nm. The level of human VEGFR-2 in samples was calculated (pg/ml) as duplicate determinations from the standard curve. Percent inhibition was calculated in comparison to control untreated cells.

5.2.2.2. In vitro effect of the synthesized compounds on VEGFR-2. Compounds **7a**, **8c**, **9b**, **9c** and **9d** were evaluated for their *in vitro* inhibitory activity against Human VEGFR-2 using ELISA kit according

to manufacturer's instructions (Ray Biotech). This assay employs an antibody specific for human VEGFR-2 coated on a 96-well plate. Samples and standards were added to the wells and incubated over night at 4 °C with gentle shaking. The wells were washed and biotinylated antibody was added followed by incubation for one hour at room temperature. After washing away unbound biotinylated antibody, HRP-conjugated streptavidin was pipetted to the wells and incubated at room temperature for 45 min. The wells were then washed; TMB substrate solution was added and incubated for 30 min. The color developed was in proportion to the amount of VEGFR-2 bound. The Stop Solution was added and the intensity of the color was measured at 450 nm. Percent inhibition was calculated by the comparison of compounds treated to control incubations. The concentration of the test compound causing 50% inhibition (IC_{50}) was calculated from the concentration inhibition response curve and the data were compared with sorafenib as standard VEGFR-2 inhibitor.

5.2.3. Cell cycle analysis of compound **9d**

The MCF-7 cells were treated with 5.41 μM of compound **9d** for 24 h. After treatment, the cells were washed twice with ice-cold phosphate buffer saline (PBS) and collected by centrifugation. The cell pellets were then fixed in ice-cold 70% (v/v) ethanol, washed with PBS and re-suspended with 0.1 mg/mL RNase. The collected cell pellets were stained with 40 mg/mL propidium iodide (PI), and analyzed by flow cytometry using FACSCalibur [60].

5.2.4. Measurement of apoptosis of **9d** using annexin-V-FITC apoptosis detection kit

Apoptosis was assessed by staining the cells with Annexin V fluorescein isothiocyanate (FITC) and counterstaining with PI using the Annexin V-FITC/PI apoptosis detection kit (BD Biosciences, San Diego, CA) according to the manufacturer's instructions. Briefly, 4×10^6 cell/T75 flask was treated with compound **9d** at its IC_{50} concentration (5.41 μM) for 24 h. The cells were collected by trypsinization and 0.5×10^6 cells were washed twice with phosphate-buffered saline (PBS) and stained with 5 μL Annexin V-FITC and 5 μL PI in 1 × binding buffer for 15 min at room temperature in the dark. Analyses were carried out using FACS Calibur flow cytometer (BD Biosciences, San Jose, CA) [60].

5.2.5. Measurement of the effect of compound **9d** on the level of p53, Bax and BCL-2

The levels of the tumor suppressor gene p53, anti-apoptotic marker BCL-2 as well as the apoptotic marker Bax were assessed using BIORAD iScriptTM One-Step RT-PCR kit with SYBR® Green. The procedure of the used kit was done according to the manufacturer's instructions [60].

5.2.6. Caspases-7 and -9 assays

Activities of caspase-7 and caspase-9 were measured using Human CASP7 (Caspase-7) ELISA Kit from MyBioSource INC. Catalog # MBS2505226 (96 tests) (MyBioSource, Inc., San Diego, CA, USA) and DRG® Caspase-9 (human) ELISA (EIA-4860) kit (DRG International Inc., USA), according to the manufacturer instructions.

5.3. Molecular modeling

5.3.1. Target preparation

The crystal structure of VEGFR-2 was retrieved from the RCSB Protein Data Bank (PDB ID: 3U6J, http://www.rcsb.org) and was selected as a target in the modeling study. Water molecules and hydrogen atoms were added and the energy of the system was minimized with MOE 2008.10 (Molecular Operating Environment, http://www.chemcomp.com).

5.3.2. Ligand preparation

The compounds were prepared with MOE 2008.10. Structures and energy minimization were carried out with MOE, the placement criterion was chosen to be the MMFF94× force field until RMSD gradient of 0.05 kcal mol^{-1} $Å^{-1}$ was reached.

5.3.3. Molecular docking

Compounds **7a**, **8c** and **9d** were docked within the ATP binding site and the allosteric site of VEGFR-2. The placement criterion was adjusted to be Triangle Matcher. Rescoring 1 was selected to be London G and Retain 30 poses. In our study we prefer to make refinement with Force field and rescoring 2 was chosen to be London G.

5.3.4. Molecular dynamics

MD was carried out using GROMACS 5.1.2 software package [61]. The topology files of 3U6J were directly created by GROMACS, whereas Acpype software [62] was used to generate topology files of the compounds **7a**, **8c** and **9d**. All the three complexes and the protein alone were immersed in the centre of cubic box with margin of 1 nm, then the boxes were filled with TIP3P water model. Sodium and chloride ions were added to neutralize the systems, then the complexes were relaxed *via* energy minimization using steepest descent minimization algorithm until the maximum force is under1000 kcal/mol/nm. The complexes were equilibrated through two steps, first one was NVT ensemble (constant Number of particles, Volume and Temperature) for 100 ps (picoseconds) to stabilize the system at 300 K, and the second step was NPT (constant Number of particles, Pressure, and Temperature) running for 100 ps. Finally, after equilibration of each system, 10 ns MD simulation was performed.

5.3.5. QSAR study

QSAR models were built by QSAR software of MOE 2008, applying builder tool. Energy minimization was performed using MMFF94x force field. The experimental IC_{50} values were converted to pIC_{50} using equation: $pIC_{50} = (-\log IC_{50})$. Different 2D and 3D descriptors were calculated such as physical descriptors, constitutional properties, quantum chemical descriptors, topological descriptors, surface area, volume and shape descriptors and molecular properties. The predicted pIC_{50} were calculated and models' validation was carried out by using the r^2, RMSE, SE and residual values between the expected and the predicted pIC_{50}.

Acknowledgments

The authors are grateful to Dr. Esam Rashwan, Head of the confirmatory diagnostic unit VACSERA-EGYPT, for carrying out the cell cycle analysis and apoptosis markers assays.

References

[1] L.A. Torre, F. Bray, R.L. Siegel, J. Ferlay, J. Lortet-Tieulent, A. Jemal, Global cancer statistics, 2012, CA Canc. J. Clin. 65 (2015) 87–108.
[2] D.E. Gerber, Targeted therapies: a new generation of cancer treatments, Am. Fam. Phys. 77 (2008) 311–319.
[3] R.S. Kerbel, Tumor angiogenesis: past, present and the near future, Carcinogenesis 21 (2000) 505–515.
[4] P.J. Polverini, The pathophysiology of angiogenesis, Crit. Rev. Oral. Biol. Med. 6 (1995) 230–247.
[5] I.J. Fidler, Angiogenesis and cancer metastasis, Canc. J. 6 (Suppl. 2) (2000) S134–S141.
[6] A.F. Karamysheva, Mechanisms of angiogenesis, Biochemistry (Mosc.) 73 (2008) 751–762.
[7] H.L. Goel, A.M. Mercurio, VEGF targets the tumour cell, Nat. Rev. Canc. 13 (2013) 871–882.
[8] J.E. Ohm, D.P. Carbone, VEGF as a mediator of tumor-associated immunodeficiency, Immunol. Res. 23 (2001) 263–272.
[9] M. Shibuya, Vascular endothelial growth factor (VEGF) and its receptor (VEGFR) signaling in angiogenesis. A crucial target for anti- and pro-angiogenic therapies, Genes Canc. 2 (2011) 1097–1105.
[10] M. Lohela, M. Bry, T. Tammela, K. Alitalo, VEGFs and receptors involved in angiogenesis versus lymphangiogenesis, Curr. Opin. Cell Biol. 21 (2009) 154–165.
[11] S. Tugues, S. Koch, L. Gualandi, X. Li, L. Claesson-Welsh, Vascular endothelial growth factors and receptors: anti-angiogenic therapy in the treatment of cancer,

Mol. Asp. Med. 32 (2011) 88–111.
[12] K. Holmes, O.L. Roberts, A.M. Thomas, M.J. Cross, Vascular endothelial growth factor receptor-2: structure, function, intracellular signalling and therapeutic inhibition, Cell Sig. 19 (2007) 2003–2012.
[13] C.V. Parast, B. Mroczkowski, C. Pinko, S. Misialek, G. Khambatta, K. Appelt, Characterization and kinetic mechanism of catalytic domain of human vascular endothelial growth factor receptor-2 tyrosine kinase (VEGFR2 TK), a key enzyme in angiogenesis, Biochemistry 37 (1998) 16788–16801.
[14] C. Fontanella, E. Ongaro, S. Bolzonello, M. Guardascione, G. Fasola, G. Aprile, Clinical advances in the development of novel VEGFR2 inhibitors, Ann. Transl. Med. 2 (2014) 123.
[15] J.Y. Hsu, H.A. Wakelee, Monoclonal antibodies targeting vascular endothelial growth factor: current status and future challenges in cancer therapy, BioDrugs 23 (2009) 289–304.
[16] P. Wu, T.E. Nielsen, M.H. Clausen, FDA-approved small-molecule kinase inhibitors, Tren. Pharmacol. Sci. 36 (2015) 422–439.
[17] H.X. Chen, J.N. Cleck, Adverse effects of anticancer agents that target the VEGF pathway, Nat. Rev. Clin. Oncol. 6 (2009) 465–477.
[18] Z. Zhao, H. Wu, L. Wang, Y. Liu, S. Knapp, Q. Liu, N.S. Gray, Exploration of type II binding mode: a privileged approach for kinase inhibitor focused drug discovery? ACS Chem. Biol. 9 (2014) 1230–1241.
[19] Y. Liu, N.S. Gray, Rational design of inhibitors that bind to inactive kinase conformations, Nat. Chem. Biol. 2 (2006) 358–364.
[20] X. Wu, S. Wan, G. Wang, H. Jin, Z. Li, Y. Tian, Z. Zhu, J. Zhang, Molecular dynamics simulation and free energy calculation studies of kinase inhibitors binding to active and inactive conformations of VEGFR-2, J. Mol. Graph. Model. 56 (2015) 103–112.
[21] M. Fasano, C.M. Della Corte, R. Califano, A. Capuano, T. Troiani, E. Martinelli, F. Ciardiello, F. Morgillo, Type III or allosteric kinase inhibitors for the treatment of non-small cell lung cancer, Exp. Opin. Investig. Drugs 23 (2014) 809–821.
[22] M.A. Abdullaziz, H.T. Abdel-Mohsen, A.M. El Kerdawy, F.A.F. Ragab, M.M. Ali, S.M. Abu-Bakr, A.S. Girgis, H.I. El Diwani, Design, synthesis, molecular docking and cytotoxic evaluation of novel 2-furybenzimidazoles as VEGFR-2 inhibitors, Eur. J. Med. Chem. 136 (2017) 315–329.
[23] N.C. Kampan, M.T. Madondo, O.M. McNally, M. Quinn, M. Plebanski, Paclitaxel and its evolving role in the management of ovarian cancer, Biomed. Res. Int. 2015 (2015) 413076.
[24] M.A. Jordan, D. Thrower, L. Wilson, Mechanism of inhibition of cell proliferation by Vinca alkaloids, Canc. Res. 51 (1991) 2212–2222.
[25] K. Fujita, Y. Kubota, H. Ishida, Y. Sasaki, Irinotecan, a key chemotherapeutic drug for metastatic colorectal cancer, World J. Gastroenterol. 21 (2015) 12234–12248.
[26] S. Ijaz, N. Akhtar, M.S. Khan, A. Hameed, M. Irfan, M.A. Arshad, S. Ali, M. Asrar, Plant derived anticancer agents: a green approach towards skin cancers, Biomed. Pharmacother. 103 (2018) 1643–1651.
[27] P. Pratheeshkumar, A. Budhraja, Y.O. Son, X. Wang, Z. Zhang, S. Ding, L. Wang, A. Hitron, J.C. Lee, M. Xu, G. Chen, J. Luo, X. Shi, Quercetin inhibits angiogenesis mediated human prostate tumor growth by targeting VEGFR- 2 regulated AKT/mTOR/P70S6K signaling pathways, PLoS One 7 (2012) e47516.
[28] A.P. Athira, C.S. Abhinand, K. Saja, A. Helen, P. Reddanna, P.R. Sudhakaran, Anti-angiogenic effect of chebulagic acid involves inhibition of the VEGFR2- and GSK-3β-dependent signaling pathways, Biochem. Cell Biol. 95 (2017) 563–570.
[29] S.Y. Park, E.H. Seo, H.S. Song, S.Y. Jung, Y.K. Lee, K.Y. Yi, S.E. Yoo, Y.J. Kim, KR-31831, benzopyran derivative, inhibits VEGF-induced angiogenesis of HUVECs through suppressing KDR expression, Int. J. Oncol. 32 (2008) 1311–1315.
[30] R.Z. Batran, D.H. Dawood, S.A. El-Seginy, T.J. Maher, K.S. Gugnani, A.N. Rondon-Ortiz, Coumarinyl pyranopyrimidines as new neuropeptide S receptor antagonists; design, synthesis, homology and molecular docking, Bioorg. Chem. 75 (2017) 274–290.
[31] O.M. Abdelhafez, K.M. Amin, H.I. Ali, M.M. Abdalla, R.Z. Batran, Synthesis of new 7-oxycoumarin derivatives as potent and selective monoamine oxidase A inhibitors, J. Med. Chem. 55 (2012) 10424–10436.
[32] R.Z. Batran, A.F. Kassem, E.M.H. Abbas, S.A. Elseginy, M.M. Mounier, Design, synthesis and molecular modeling of new 4-phenylcoumarin derivatives as tubulin polymerization inhibitors targeting MCF-7 breast cancer cells, Bioorg. Med. Chem. 26 (2018) 3474–3490.
[33] N.A. Abdel Latif, R.Z. Batran, M.A. Khedr, M.M. Abdalla, 3-Substituted-4-hydroxycoumarin as a new scaffold with potent CDK inhibition and promising anticancer effect: synthesis, molecular modeling and QSAR studies, Bioorg. Chem. 67 (2016) 116–129.
[34] R.Z. Batran, D.H. Dawood, S.A. El-Seginy, M.M. Ali, T.J. Maher, K.S. Gugnani, A.N. Rondon-Ortiz, New coumarin derivatives as anti-breast and anti-cervical cancer agents targeting VEGFR-2 and p38α MAPK, Arch. Pharm. (Weinheim) 350 (2017) e1700064.
[35] G. Luo, X. Li, G. Zhang, C. Wu, Z. Tang, L. Liu, Q. You, H. Xiang, Novel SERMs based on 3-aryl-4-aryloxy-2H-chromen-2-one skeleton – a possible way to dual ERα/VEGFR-2 ligands for treatment of breast cancer, Eur. J. Med. Chem. 140 (2017) 252–273.
[36] S.L. Park, S.Y. Won, J.H. Song, S.Y. Lee, W.J. Kim, S.K. Moon, Esculetin inhibits VEGF-induced angiogenesis both in vitro and in vivo, Am. J. Chin. Med. 44 (2016) 61–76.
[37] M.H. Jung, S.H. Lee, E.M. Ahn, Y.M. Lee, Decursin and decursinol angelate inhibit VEGF-induced angiogenesis via suppression of the VEGFR-2-signaling pathway, Carcinogenesis 30 (2009) 655–661.
[38] R. Pan, Y. Dai, X.H. Gao, D. Lu, Y.F. Xia, Inhibition of vascular endothelial growth factor-induced angiogenesis by scopoletin through interrupting the autophosphorylation of VEGF receptor 2 and its downstream signaling pathways, Vascul. Pharmacol. 54 (2011) 18–28.
[39] M.Y. Zhao, Y. Yin, X.W. Yu, C.B. Sangani, S.F. Wang, A.M. Lu, L.F. Yang, P.C. Lv, M.G. Jiang, H.L. Zhu, Synthesis, biological evaluation and 3D-QSAR study of novel 4,5-dihydro-1H-pyrazole thiazole derivatives as BRAF($V^{600}E$) inhibitors, Bioorg. Med. Chem. 23 (2015) 46–54.
[40] D. Havrylyuk, B. Zimenkovsky, O. Vasylenko, A. Gzella, R. Lesyk, Synthesis of new 4-thiazolidinone-, pyrazoline-, and isatin-based conjugates with promising antitumor activity, J. Med. Chem. 55 (2012) 8630–8641.
[41] H.H. Wang, K.M. Qiu, H.E. Cui, Y.S. Yang, Xing M Yin-Luo, X.Y. Qiu, L.F. Bai, H.L. Zhu, Synthesis, molecular docking and evaluation of thiazolyl-pyrazoline derivatives containing benzodioxole as potential anticancer agents, Bioorg. Med. Chem. 21 (2013) 448–455.
[42] P.C. Lv, D.D. Li, Q.S. Li, X. Lu, Z.P. Xiao, H.L. Zhu, Synthesis, molecular docking and evaluation of thiazolyl-pyrazoline derivatives as EGFR TK inhibitors and potential anticancer agents, Bioorg. Med. Chem. Lett. 21 (2011) 5374–5377.
[43] K.M. Qiu, H.H. Wang, L.M. Wang, Y. Luo, X.H. Yang, X.M. Wang, H.L. Zhu, Design, synthesis and biological evaluation of pyrazolyl-thiazolinone derivatives as potential EGFR and HER-2 kinase inhibitors, Bioorg. Med. Chem. 20 (2012) 2010–2018.
[44] O.O. Ajani, O.C. Nwinyi, Microwave-assisted synthesis and evaluation of antimicrobial activity of 3-{3-(s-aryl and s-heteroaromatic)acryloyl}-2H-chromen-2-one derivatives, J. Heterocyc. Chem. 47 (2010) 179–187.
[45] N. Hamdi, C. Fischmeister, M.C. Puerta, P. Valerga, A rapid access to new coumarinyl chalcone and substituted chromeno[4,3-c]pyrazol-4(1H)-ones and their antibacterial and DPPH radical scavenging activities, Med. Chem. Res. 20 (2011) 522–530.
[46] S. Guo, L.S. Colbert, M. Fuller, Y. Zhang, R.R. Gonzalez-Perez, Vascular endothelial growth factor receptor-2 in breast cancer, Biochim. Biophys. Acta. 1806 (2010) 108–121.
[47] L.F. Brown, B. Berse, R.W. Jackman, K. Tognazzi, A.J. Guidi, H.F. Dvorak, D.R. Senger, J.L. Connolly, S.J. Schnitt, Expression of vascular permeability factor (vascular endothelial growth factor) and its receptors in breast cancer, Hum. Pathol. 26 (1995) 86–91.
[48] K.C. Zimmermann, D.R. Green, How cells die: apoptosis pathways, J. Aller. Clin. Immunol. 108 (4 Suppl.) (2001) S99–S103.
[49] A. Frenzel, F. Grespi, W. Chmelewskij, A. Villunger, Bcl2 family proteins in carcinogenesis and the treatment of cancer, Apoptosis 14 (2009) 584–596.
[50] T. Miyashita, S. Krajewski, M. Krajewska, H.G. Wang, H.K. Lin, D.A. Liebermann, B. Hoffman, J.C. Reed, Tumor suppressor p53 is a regulator of bcl-2 and bax gene expression in vitro and in vivo, Oncogene 9 (1994) 1799–1805.
[51] A.B. Parrish, C.D. Freel, S. Kornbluth, Cellular mechanisms controlling caspase activation and function, Cold Spr. Harb. Perspect. Biol. 5 (2013) pii: a008672.
[52] J. Zhang, P.L. Yang, N.S. Gray, Targeting cancer with small molecule kinase inhibitors, Nat. Rev. Canc. 9 (2009) 28–39.
[53] D. Bauer, D.A. Whittington, A. Coxon, J. Bready, S.P. Harriman, V.F. Patel, A. Polverino, J.C. Harmange, Evaluation of indazole-based compounds as a new class of potent KDR/VEGFR-2 inhibitors, Bioorg. Med. Chem. Lett. 18 (2008) 4844–4848.
[54] T. Honda, H. Nagahara, H. Mogi, M. Ban, H. Aono, KDR inhibitor with the intramolecular non-bonded interaction: conformation-activity relationships of novel indole-3-carboxamide derivatives, Bioorg. Med. Chem. Lett. 21 (2011) 1782–1785.
[55] D.M. Sammond, K.E. Nailor, J.M. Veal, R.T. Nolte, L. Wang, V.B. Knick, S.K. Rudolph, A.T. Truesdale, E.N. Nartey, J.A. Stafford, R. Kumar, M. Cheung, Discovery of a novel and potent series of dianilinopyrimidineurea and urea isostere inhibitors of VEGFR2 tyrosine kinase, Bioorg. Med. Chem. Lett. 15 (2005) 3519–3523.
[56] Molecular Operating Environment. < http://www.Chemcomp.com > .
[57] G. Cruciania, P. Crivorib, P.-A. Carruptb, B. Testab, Molecular fields in quantitative structure–permeation relationships: the VolSurf approach, J. Mol. Struct. (THEOCHEM) 503 (2000) 17–30.
[58] P. Skehan, R. Storeng, D. Scudiero, A. Monks, J. McMahon, D. Vistica, J.T. Warren, H. Bokesch, S. Kenney, M.R. Boyd, New colorimetric cytotoxicity assay for anticancer-drug screening, J. Natl. Canc. Inst. 82 (1990) 1107–1112.
[59] M.M. Ali, A.E. Mahmoud, A.H. Abdel-Halim, A.A. Fyiad, Anti-cancer effect of some prepared sulfated oligosaccharides on three different human cancer cell lines, Asian J. Pharmaceut. Clin. Res. 7 (2014) 168–176.
[60] E.F. Abdelhaleem, M.K. Abdelhameid, A.E. Kassab, M.M. Kandeel, Design and synthesis of thienopyrimidine urea derivatives with potential cytotoxic and pro-apoptotic activity against breast cancer cell line MCF-7, Eur. J. Med. Chem. 143 (2018) 1807–1825.
[61] M.J. Abraham, D. van der Spoel, E. Lindahl, B. Hess, the GROMACS Development Team, GROMACS User Manual version 5.1.2, 2016. < www.gromacs.org > .
[62] A.W. Sousa da Silva, W.F. Vranken, ACPYPE -AnteChamber PYthon Parser interfacE, BMC Res. Notes 5 (2012) 367.